Rock Glacier Inventory, Permafrost Probability Distribution Modeling and Associated Hazards in the Hunza River Basin, Western Karakoram, Pakistan

Article *in* Science of The Total Environment · March 2021

DOI: 10.1016/j.scitotenv.2021.146833

CITATIONS
0

READS
100

4 authors:

Javed Hassan
Chinese Academy of Sciences
5 PUBLICATIONS **25** CITATIONS
SEE PROFILE

Xiaoqing Chen
Chinese Academy of Sciences
51 PUBLICATIONS **443** CITATIONS
SEE PROFILE

Sher Muhammad
International Centre for Integrated Mountain Development
46 PUBLICATIONS **404** CITATIONS
SEE PROFILE

Nazir Ahmed Bazai
Chinese Academy of Sciences
17 PUBLICATIONS **20** CITATIONS
SEE PROFILE

Science of the Total Environment 782 (2021) 146833

Contents lists available at ScienceDirect

Science of the Total Environment

journal homepage: www.elsevier.com/locate/scitotenv

Rock glacier inventory, permafrost probability distribution modeling and associated hazards in the Hunza River Basin, Western Karakoram, Pakistan

Javed Hassan [a,c], Xiaoqing Chen [a,b,c,*], Sher Muhammad [d], Nazir Ahmed Bazai [a,c,e]

[a] Key Laboratory of Mountain Hazards and Earth Surface Process, Institute of Mountain Hazards and Environment, Chinese Academy of Sciences, Chengdu 610041, China
[b] CAS Centre for Excellence in Tibetan Plateau Earth Sciences, Beijing 100101, China
[c] University of Chinese Academy of Sciences, Beijing 100049, China
[d] International Center for Integrated Mountain Development (ICIMOD), Kathmandu, Nepal
[e] China-Pakistan Joint Research Center on Earth Science, QAU, Islamabad, Pakistan

HIGHLIGHTS

- The first complete rock glacier inventory for the Hunza Basin has been generated and compiled.
- The categorized rock glacier inventory is used to model permafrost probability distribution.
- Rock glacier destabilization is further analysed for 68 rock glaciers that interacted with river channels.
- Rock glacier and permafrost variation can cause cryospheric hazards with substantial damages.

GRAPHICAL ABSTRACT

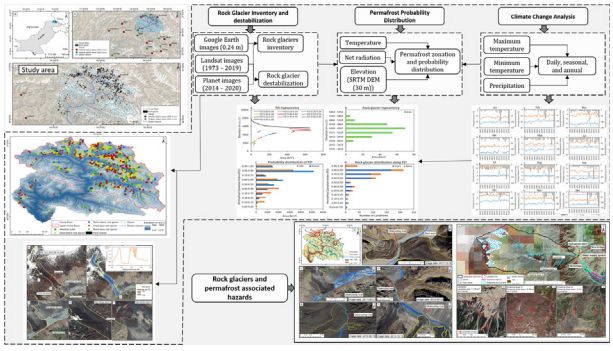

ARTICLE INFO

Article history:
Received 21 December 2020
Received in revised form 24 March 2021
Accepted 25 March 2021
Available online 30 March 2021

Editor: A P Dimri

Keywords:
Rock glaciers
Permafrost
Karakoram
Cryospheric hazards
Climate change

ABSTRACT

The destabilization of rock glaciers and permafrost variations is of great importance to the safety of the population and infrastructure in the Karakoram region because of their effects on land stability and river obstructions. In this study, we compiled the first complete rock glacier inventory for the Hunza Basin, western Karakoram, of 616 rock glaciers with an area of 194 km^2 between 2800 and 5700 m a.s.l. We categorized the rock glaciers as intact or relict, and their distributions and destabilization were further analyzed and used along with in situ climate and elevation dataset to model the permafrost probability distribution. The modeled areas where the permafrost zonation index (PZI) is 0.5–1.00 indicate that permafrost occurs over 85% of the catchment area and lies above 3525 m a.s.l., which closely matches the zero-degree isotherm of 3800 m a.s.l. Based on the sensitivity analysis of the independent variables, elevation is the most sensitive variable, followed by net radiation, for predicting the probabilities of the presence and absence of permafrost. The model distributions are quite precise, with median posterior areas under the curve of 0.98 and 0.96 for model training and testing, respectively. We analyzed the rock glacier destabilization for 68 rock glaciers that interacted with river channels, of which 50 blocked or diverted river channels. Destabilized rock glaciers can be closely linked to the 0 °C isotherm between 3400 and 4600 m a.s.l. The significant damage caused by periodic floods from the subsequent blockage of river channels by landslides can be attributed to variations in permafrost. Which demolished infrastructure, including a hydropower plant, suspension bridge and water supply system in Hassan-abad catchment. Quantification of rock glacier dynamics and permafrost in the region can further improve policies related to the reduction in disaster risk and mitigation of associated hazards.

* Corresponding author at: Key Laboratory of Mountain Hazards and Earth Surface Process, Institute of Mountain Hazards and Environment, Chinese Academy of Sciences, Chengdu 610041, China.
E-mail addresses: xqchen@imde.ac.cn (X. Chen), sher.muhammad@icimod.org (S. Muhammad).

https://doi.org/10.1016/j.scitotenv.2021.146833
0048-9697/

1. Introduction

Rock glaciers and permafrost are important components of the cryosphere, and debris-covered rock glaciers are allegedly more climate resilient than debris-free and debris-covered glaciers (Anderson et al., 2018; Jones et al., 2021; Jones et al., 2019b). Rock glaciers are frozen mixtures of rock debris and ice that can accumulate and deform under the influence of gravity to form striking tongue-shaped features with surface structures resembling viscous flow (Barsch, 1996; Elizabeth Martin and Whalley, 1987; Haeberli, 1985; Kääb et al., 2020). Rock glaciers typically move a few centimeters to meters per year (Kääb et al., 2003; Kääb et al., 2020). Rock glaciers are abundant in the Karakoram region of northern Pakistan and exhibit morainic and portals nature restricted altitudinally and climatically to certain geographical locations (Jones et al., 2019a; Owen and England, 1998; Schmid et al., 2015). Permafrost variation and rock glaciers interaction with river channel possess potentially threats to the infrastructure and development (Blöthe et al., 2019; Schmid et al., 2015). Slope failures, rockfalls and ground subsidence following deglaciation in mountainous regions are frequently recognized (Beniston et al., 2018; Harrison, 2009; Jones et al., 2019a; Knight and Harrison, 2014; Schmid et al., 2015).

A large proportion of the global permafrost is situated in mountainous terrains (Gruber, 2012), including the densely populated areas of High Mountain Asia (HMA) (Gruber et al., 2017; Schmid et al., 2015). Rock glacier dynamics and the permafrost distribution in the Karakoram region have not been thoroughly investigated, and there has been no systematic collection of rock glacier and permafrost data in the Karakoram region (Ipcc et al., 2019; Wester et al., 2019), while glacier dynamics and the impacts of climate change are relatively well investigated (Azam et al., 2018; Bocchiola and Soncini, 2019; Forsythe et al., 2017; Lutz et al., 2014; Lutz et al., 2016; Muhammad et al., 2019a; Muhammad et al., 2019b). Studies of the distribution of permafrost and permafrost changes are mostly conducted on the Tibetan Plateau because of the consequences of permafrost degradation on infrastructural development (Jin et al., 2000; Wang and French, 1994; Yang et al., 2004). Previous studies of rock glaciers and permafrost in the Himalayas were limited to certain confined regions (Allen et al., 2016; Mayewski et al., 1981; Owen and England, 1998). Rock glaciers in the Hindu Kush Himalaya (HKH) region are reported to be distributed between ~3554 m a.s.l. in northern Afghanistan and ~ 5735 m a.s.l. on the Tibetan Plateau (Schmid et al., 2015). An inventory of 1004 rock glaciers in Uttarakhand State, India, presented by Baral et al. (2020) revealed that terrain aspect and elevation (> 4000 m a.s.l.) significantly control the distribution of rock glaciers. Jones et al. (2019b) showed the hydrological significance of rock glaciers as nonnegligible long-term water stores, particularly in deglaciating and glaciated semiarid and arid regions. Rock glacier hydrology is a curtail controlling parameter of temperature and velocity, with annual air temperature and snow cover as external forcing parameters (Delaloye et al., 2013; Ikeda et al., 2008; Kenner et al., 2020). Moreover, the rock glacier creep rate is more likely controlled by the hydrological processes (Buchli et al., 2017). The hydrological contributions from rock glaciers to future climate change and the degradation of glaciers may increase in downstream regions.

Recently, few studies have been conducted to assess the rock glaciers and permafrost in the western HKH and Pamir regions. Among which Kääb et al. (2020) presented an inventory to evaluate rock glacier dynamics and found increasing surface velocities since the 1950s for selected rock glaciers in the Ile Alatau and Kungöy Ala-Too ranges of the northern Tien Shan. Rock glaciers in the northern Tien Shan originated from within the permafrost zone, and some large rock glaciers flow down to elevations where permafrost is unlikely to exist (Bolch and Gorbunov, 2014). Jones et al. (2021) estimated (51.80 ± 10.36 water volume equivalents) for ~25,000 landforms in Himalayan region and the relative hydrological importance of rock glaciers is likely to increase in future.

Despite negative global glacier mass budget anticipated by global climate change for rest of the world (Farinotti et al., 2019; Nie et al., 2021; Huss and Hock, 2015; Huss and Hock, 2018), in the Karakoram region, most of the cryospheric studies have found glacier mass balance anomalies, with insignificant losses of glacier mass or balanced glacier mass budgets in recent years (Azam et al., 2018; Berthier and Brun, 2019; Kääb et al., 2012; Muhammad et al., 2019b; Yao et al., 2012; Muhammad and Tian, 2016). An improved understanding of the cryospheric changes (including permafrost and rock glaciers) within the HKH region is important because of its large area (3746.77 km^2 (Jones et al., 2021)) and dense population (Schmid et al., 2015). Global climate change is likely to impact rock glaciers destabilization and permafrost, which could affect slope destabilization, landslides, debris flows, vegetation changes, run-off patterns, and water qualities.

Primary objective of the current study is to develop a first systematic complete rock glacier inventory and analyze destabilization of the rock glacier in the Karakoram which interacted with river channel. The categorized rock glacier inventory is further use to model the permafrost probability distribution in the Hunza Basin to address the potential for associated geohazards. The rock glacier distribution and destabilization along with long-term surface velocities between 1973 and 2019 is evaluated to analyze the rock glaciers destabilization. Additionally, the predicted permafrost zone boundaries are used to predict slope destabilizations and the damage caused by periodic landslide-induced floods. Field evidence presented in the current research demonstrates the importance of the evolution of paraglacial landforms for the consideration of safety, implementation of water management projects, development and planning of infrastructure and other socioeconomic reasons. Therefore, we argue that the quantification of the geohazards associated with rock glacier destabilization and spatiotemporal variations in permafrost is crucial. This can further inform policies regarding water management, infrastructure planning and also support future cryosphere and downstream impact studies in the Karakoram region.

2. Material and methods

2.1. Study area

The Hunza Basin is located in the western Karakoram, Pakistan, with an area of 13,713 km^2 between 36.05 and 37.08°N and 74.04–75.77°E (Fig. 1). The minimum elevation in the Hunza Basin is 1432 m a.s.l. at Danyore Bridge, and the maximum elevation is 7849 m a.s.l. at the summit of Mount Rakaposhi in the northeastern part of the catchment. The Hunza Basin is one of the most heavily glaciated catchments in the Karakoram region: approximately 30% of the entire catchment area is glaciated, and 16% of the glaciated area is debris-covered ice (Consortium, 2017). The heavily glaciated terrain of the Hunza Basin and its mean elevation of 4631 m a.s.l. make it conducive to hosting permafrost in a large portion of the catchment (Gruber, 2012). Mapping by Schmid et al. (2015) in the Karakoram region indicated that the lowest elevations of active rock glaciers were between 3850 and 5100 m a.s.l. The terminuses of some inactive rock glaciers reached even lower elevations (3350 m a.s.l.) in the western Karakoram (Hewitt, 2014).

The regional climate of the Karakoram is affected by two prevailing weather patterns, the winter westerlies and the Indian monsoon, with great microclimatic variability due to the high mountain terrain (Bolch et al., 2012; Hewitt et al., 1989). The climate of the Hunza Basin is dominated by precipitation from the winter westerlies (Bocchiola and Soncini, 2019; Immerzeel et al., 2015; Shrestha et al., 2015). According to the Köppen climate classification, the Hunza Basin lies in a "cold desert" with low precipitation and significant daily temperature variations (Bocchiola and Soncini, 2019). The summer monsoon contributes little precipitation (only 27% of the annual precipitation during summer months) to the Hunza Basin, unlike in the central Himalayas, where 90% of the annual precipitation falls during June–September (Hassan et al., 2017; Jones et al., 2019a; Khadka et al., 2020). A map of the

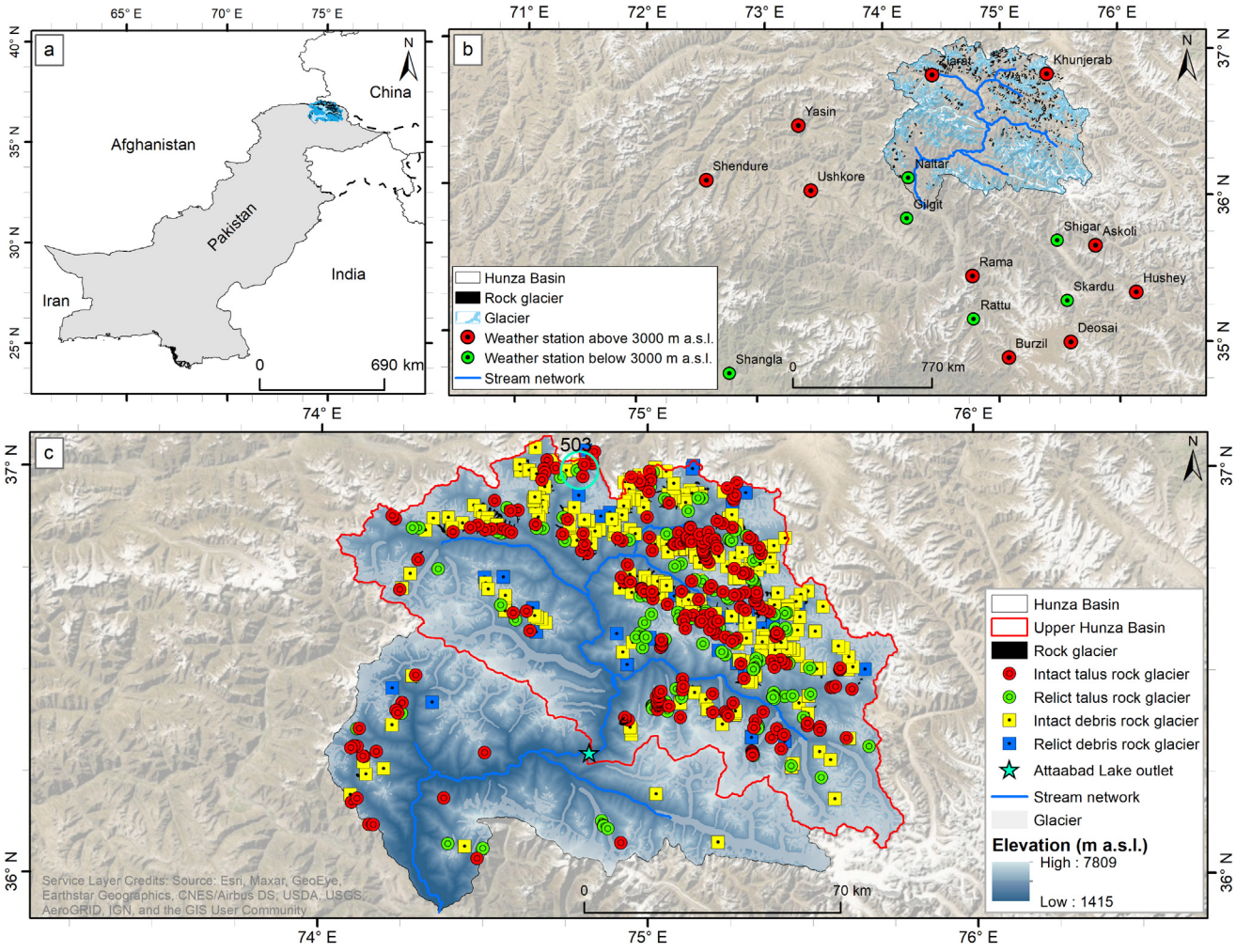

Fig. 1. (a) The Hunza Basin is located in northern Pakistan near the Pakistan-China border. (b) The red circles represent the weather stations located above 3000 m a.s.l., and the green circles represent the low-elevation weather stations used in the current study. (c) The spatial distributions of categorized rock glaciers red (intact talus rock glacier), green (relict talus rock glaciers), yellow (intact debris rock glaciers), and blue (intact debris rock glaciers). Glaciers in the catchment are shown in light gray. The outlet of Attaabad Lake is indicated by the green star, with the stream network indicated by blue lines. Location of one of the destabilized rock glaciers discussed in Section 3.2 is highlighted by blue circle. (For interpretation of the references to color in this figure legend, the reader is referred to the web version of this article.)

study area in the Karakoram region is shown in Fig. 1 along with the rock glacier inventory that was developed in this study.

2.2. Meteorological datasets and climate change trend analysis

Daily meteorological datasets including near-surface air temperature, radiation and precipitation from 1995 to 2019 were collected from low- and high-elevation meteorological stations established by the Pakistan Water and Power Development Authority (WAPDA), Pakistan Glacier Monitoring Research Centre-Water and Power Development Authority (GMRC-WAPDA) and Pakistan Meteorological Department. Data from 16 weather stations are included in the current study for analysis. Climate change trend analysis is carried out using the obtained datasets from each station, categorized based on whether the altitudes of the meteorological stations are above or below 3000 m a.s.l. (Fig. 1b). A nonparametric Mann-Kendall (MK) test is performed to assess the significance of meteorological variations in the stations on daily, seasonal and annual bases. Climate data from the three meteorological stations located within the Hunza Basin are also used to estimate the zero-degree isotherm during 1995–2019. The long-term in situ measured meteorological data are distributed using the local lapse rates estimated between the individual stations. The spatially distributed meteorological data between 1995 and 2019 are also used to estimate the permafrost probability distribution, including the rock glacier inventory as the dependent variable. The long-term spatiotemporal meteorological datasets significantly reduce the uncertainties in the climate change trend analysis and models of the permafrost probability distribution. In addition, field work was conducted from 7 to 8 September 2020 to assess the damages caused by landslides and floods in the Hassan-abab catchment located within Hunza Basin.

2.3. Satellite images and digital elevation model

High resolution satellite images form Planet (3 m) and Landsat images of TM, ETM and OLI/TIRS (30 m) with minimum cloud cover (≤20%) and snow cover were used for estimation of surface velocity and determination of rock glacier stability. The minimum snow cover extent is expected from August to October in the Karakoram region. Due to the lack of quality Landsat images for certain dates, we used the minimum snow and cloud cover images from the late ablation season. Preprocessed void-free Shuttle Radar Topography Mission (SRTM) digital elevation model (DEM) v4.1 from the Consultative Group on International Agricultural Research–Consortium for Spatial Information (CGIAR-CSI) is used in this study. The elevation data extracted from the SRTM DEM are used as one of the independent variables to estimate the permafrost probability distribution. Additional information on the Landsat images, digital elevation model and Planet images used in the current study is provided in Table S1, S2, respectively.

2.4. Rock glacier inventory

An inventory of rock glaciers is compiled by visual analysis of high-resolution (0.24 m) Google Earth images and satellite images from Planet (3 m) for the entire Hunza Basin. The satellite images used in the current study were from between 2000 and 2020. Rock glaciers in the catchment are identified based on the geomorphological evidence (i.e. front, lateral margins, and ridges-and-furrow surface topography) (Brardinoni et al., 2019; Delaloye et al., 2018) and longitudinal and Transverse flow structures (Jones et al., 2017). The approach to delineating rock glaciers in the current study was adopted from previous studies (Baral et al., 2020; Jones et al., 2017; Rangecroft et al., 2014; Schmid et al., 2015) and revised following the recommended footprints by International Permafrost Association (IPA) action group rock glaciers inventories and kinematics (Delaloye et al., 2018). The boundary of each rock glacier was digitized from the origin (root zone) of the rock glacier to the terminal front slope (foot zone). The root zone is the area where the mixture of ice and debris is created, and due to oversaturation with ice, permafrost creep starts generating the rock glacier (Barsch, 1996). Morphological dissection of the rock glacier into geomorphic zones; the upper erosional zone, (sediment supplied from a headwall) and lower depositional zone (sediment transfer and storage coexist in different proportions) can further improve the rock glacier boundaries (Brardinoni et al., 2019). The upper boundary of the rock glacier is delineated at the base of the feeding headwall. Few slopes, the boundary is extended along margins of creeping features (ridge-and-furrow topography) appeared from the ridge downslope characterized by the surface flow structures (Kääb and Weber, 2004) (For example: rock glacier ID 17 appeared to creeping downslope near up to the ridge which is also complemented by surface velocity using high resolution (3 m), multi-temporal Planet's satellite images. The lower end of the rock glacier terminates with gentle to steep slope or in few cases the unclear slope termination is attributed in the certainty index (Table S5). Rock glaciers that originated from lateral and terminal glacial moraines also include the transitional upper boundary of the rock glacier with the moraine due to overlap with the root zone. Based on visual inspection, tributary rock glaciers that merged into a single glacier were digitized as a single entity when the boundaries between them could not be correctly identified. Cloud cover, the presence of snow and image quality can introduce uncertainties in the accuracy of the inventory. We categorized the mapped landforms and built a certainty index following (Jones et al., 2017) (Table 1). The certainty index presented in Table 1 is included within the attribute of each digitized rock glacier. Which comprise of the degree of certainty over the geomorphological evidence for each rock glacier. Including the certainty index within each of the digitized polygons has largely reduced the uncertainties in the identification and categorization of rock glaciers. Availability of the multi-temporal and multi-source imagery between 2000 and 2020 has been critical for reducing uncertainty due to snow cover, cloud, and shadow. The certainty index for each digitized rock glacier is presented in Table S5. Rock glaciers with an area less than 0.01 km^2 are excluded in our inventory as per the recommendation of minimum rock glacier size by IPA action group rock glaciers inventories and kinematics (Delaloye et al., 2018). Landforms that were mapped as polygons but could not be categorized as rock glaciers based on visual inspection were not included in the inventory. Such landforms were digitized and recorded only for future reference.

Each of the digitized rock glacier polygons is named after its associated catchment (e.g., RockGlacier_Hunza appears as RG_Hnz) followed by the Google Earth image date and rock glacier identification number (e.g., RG_Hnz_YYYY-MM-DD_ID). A number of large rock glaciers in the Hunza Basin flow down to the valley floor and interact with river channels, which has also been reported in other regions of the Karakoram and Pamir (Bolch and Gorbunov, 2014; Kääb et al., 2020; Schmid et al., 2015). Multitemporal satellite images from 1973 to 2019 are used to monitor and analyze the formation of rock glacier dams created by the interactions of rock glaciers with river channels. This is critical for the quantification of the potential hazards associated with the formation and dynamics of rock glaciers.

2.5. Destabilized rock glaciers and surface velocities

The morphology of destabilized rock glacier is capable to preserve for a long time. Destabilized rock glacier showed wide variety of geomorphological features depending on degree of kinematics (Buchli et al., 2017; Delaloye et al., 2018; Marcer et al., 2019). We observed the morphological characteristic i.e. cracks, crevasses, and scarps (Marcer et al., 2019) along with the surface velocity between 1973 and 2019 and rock glacier water dam features to analyze the rock glacier destabilization and potential associated hazards. Cracks can be characterized as the shallow cuts on the surface of an active rock glacier where a strain is applied. While crevasses can be characterized by the deep incisions with a varying length and width on the rock glacier surface. Scarps are associated with deep shear planes that disconnect the rock glacier that creep at different rates (Delaloye et al., 2008; Marcer et al., 2019; Scotti et al., 2017). These surface features of rock glaciers are associated with a sudden acceleration of the portion shown in Fig. 3. Whereas identification of surface disturbance features and assign rating to entire study area of 13,713 km^2 is challenging therefore, we performed a detailed analysis of rock glacier destabilization for 68 rock glaciers which interacted with river channels. Details of the destabilized rock glacier features that could be observed from high resolution multi-temporal and multi-source satellite images are labeled and provided in Table 2.

We analyzed the surface velocity of rock glaciers in the catchment using Landsat images from between 1973 and 2019 on a decadal scale using co-registration of optically sensed images and correlation (COSI-Corr) (Leprince et al., 2007). The estimated surface velocities are further used to determine the rock glacier destabilization. COSI-Corr is widely used to estimate ground displacements and deformations and was initially designed to detect tectonic movements and deformations through the processing of optical imagery (Ayoub et al., 2009; Leprince et al., 2007). Several recent studies have used COSI-Corr to estimate glacier surface velocities (Copland et al., 2009; Sattar et al., 2019; Scherler et al., 2008). The two-step image correlation processing technique in COSI-Corr performs coregistration and correlation of multiple features by calculating displacements (Ayoub et al., 2009; Leprince et al., 2007; Steiner et al., 2018). The first step determines the shifts between images from their correlation matrixes at a multipixel scale. The second step refines the measurements at a subpixel scale with phase correlations, which rely on the Fourier shift theorem. COSI-Corr was designed to retrieve subpixel displacements between optical images, which yields an accuracy of one-fourth of a pixel (Ayoub et al., 2009; Leprince et al., 2007). In the current study, orthorectified Landsat images with minimum cloud and snow cover for the Hunza Basin between

Table 1
The certainty index (Jones et al., 2017) applied to each digitized rock glacier is presented in the rock glacier inventory in Table S4.

Parameter	Parameter options (index code)		
	1 point	2 points	3 points
External boundary	None (ON)	Vague (OV)	Clear (OC)
Snow coverage	Snow (SS)	Partial (SP)	None (SN)
Longitudinal flow structure	None (LN)	Vague (LV)	Clear (LC)
Transverse flow structure	None (TN)	Vague (TV)	Clear (TC)
Front slope	Unclear (FU)	Gentle (FG)	Steep (FS)
Certainty index score	Medium certainty (MC) ≤ 5	High certainty (HC) 6 to 10	Virtual certainty (VC) ≥ 10

Table 2
Details of the surface disturbance features observed to identify the rock glacier destabilization. Description of the cracks, crevasses and scarps is given in (Marcer et al., 2019).

Parameter	Parameter options (index code)		
	1 point	2 points	3 points
Cracks	None (CR)	Vague (CR)	Clear (CR)
Crevasses	None (CV)	Vague (CV)	Clear (CV)
Scarps	None (SC)	Vague (SC)	Clear (SC)
Surface velocity and	Between 1973 and 2019	Between 1973 and 2019	Between 1973 and 2019
Rock glacier water dam features	None	Vague	Clear

1973 and 2019 are used. For the 60 m bands of the Landsat MSS data, we used an initial statistical correlation window size of 128 × 128 pixels and a final window size of 64 × 64 pixels, with a frequency correlation engine and 2 pixels for both the X and Y steps. For the 30 m bands of the Landsat 5 MSS data, we used window sizes of 32 × 32 pixels and 16 × 16 pixels. For the data from Landsat 7 and 8, we used 64 × 64- and 32 × 32-pixel windows, with a step size setting of 4 pixels. We implemented a non-linear means filter (Ayoub et al., 2009) in COSI-Corr for noise reduction. A mask threshold of 0.9 for noise reduction is used for all correlations. This approach produces north-south and east-west displacement components that are further used to estimate the resultant surface velocities. The obtained surface velocities are filtered to remove residual altitude effects and miscorrelations (Schurer et al., 2017). We calculated the root mean squared errors (RMSEs) of the obtained velocities. We also estimated the rock glacier surface velocity using Planet images for the same overlapping period with the Landsat images to verify the surface velocity obtained using long-term Landsat images.

2.6. Permafrost probability distribution

Rock glaciers also indicates the presence of alpine permafrost and are used to map permafrost probability distributions. We performed binary logistic regression modeling using a machine learning algorithm in the Python programming language to estimate the spatial distribution of permafrost probability. Binary logistic regression models estimate the conditional probability of the dichotomous variable (Y) for the occurrence (1) and nonoccurrence (0) of permafrost depending on the set of independent variables (X_n) (Peng and So, 2002). A logistic regression model can be expressed as Eq. (1):

$$P(Y=1)=\frac{1}{1+e^{-(\beta_0+\sum\beta_n X_n)}} \quad (1)$$

where $P(Y=1)$ is the probability of outcome Y taking the value 1, β_0 is the intercept, and β_n is the regression coefficient of the independent variable X_n and is considered a predictor for the outcome Y. e is the base of the natural logarithm.

This method has been found to be appropriate and has been applied in several studies around the globe (Azócar et al., 2017; Boeckli et al., 2012; Marcer et al., 2017; Sattler et al., 2016), including the central Himalayan region (Baral et al., 2020; Haq and Baral, 2019). We used the inventory of categorized rock glaciers as the dependent variable, thus assuming that the rock glaciers are indirect indicators of permafrost. Spatially distributed local topo-climatic data, i.e., the elevations, mean annual near-surface air temperatures and net radiations derived from the meteorological stations (Fig. 1b), are used as the independent variables. Because of the collinearity between precipitation and net radiation, we did not use precipitation for the permafrost probability distribution modeling. The use of the long-term meteorological datasets enables the identification of the effects of climate change on the present-day permafrost probability distribution and has largely reduced the model uncertainties. The use of long-term meteorological data is also expected to overcome the impacts of individual meteorological events on our results. The mean annual near-surface air temperatures and net radiations are interpolated and extrapolated over the study area using the data from all 16 weather stations, and samples from raster maps at each selected rock glacier location are treated as predictor variables. To avoid coregistration errors, we projected the raster datasets to the WGS 84/UTM Zone 43 N coordinate system, and all datasets were resampled at the same spatial resolution (30 m). Point locations of the root zones of relict and intact rock glaciers are considered for modeling the permafrost probability distribution. We adopted a strategy for classifying rock glaciers into intact and relict rock glacier systems following Scotti et al. (2013) based on the morphological classification presented by Barsch (1996). We categorized rock glaciers based on whether their sediment sources were talus or glacial debris, following Scotti et al. (2013). When the sediment source is identified as glacial moraine debris, the rock glacier is classified as a debris rock glacier; when the sediment source is identified as talus, the rock glacier is classified as a talus rock glacier. The intact group of rock glaciers consists of both active and inactive rock glaciers. Active rock glaciers usually have steep fronts and side slopes, and their upper surfaces normally are covered by boulders and have furrow-and-ridge microrelief. The surface features of active rock glaciers appear to be ductile flow structures. Due to the presence of abundant ice in active rock glaciers, they have slightly higher velocities than inactive rock glaciers. Inactive rock glaciers are dynamically inactive and do not show any significant flow. Ice that might exist at the core of the frozen debris mass is protected by extensive debris cover. The mobility of an inactive rock glacier could be restrained due to a decrease in the concentration of ice (Scotti et al., 2013). Relict rock glaciers are defined as previously active landforms. On relict rock glaciers, collapsed surface structures are abundant due to the removal of ice, and the surface relief of relict rock glaciers is much more subdued than that of intact rock glaciers (Scotti et al., 2013). The estimation of rock glacier surface velocities from 1973 to 2019 has improved our categorization of active and inactive rock glaciers. Along with the surface characteristics, the surface velocities are also carefully considered. Rock glaciers displaying mean surface velocities greater than 1 m a^{-1} are classified as active rock glaciers, while those with surface velocities less than 1 m a^{-1} are classified as inactive rock glaciers. Based on the surface characteristics and degrees of activity, we classified the rock glaciers into four categories: intact talus rock glaciers, relict talus rock glaciers, intact debris rock glaciers and relict debris rock glaciers. We assumed that intact rock glaciers indicated the existence of permafrost, while relict rock glaciers indicated the absence of permafrost.

The model was then trained to evaluate the correlations between the indicators of permafrost existence, using the categorized rock glacier inventory as the dependent variable and the topo-climatic indicators as the independent variables. The method adopted here based on the rock glacier inventory and topo-climatic indicators predicts the likelihood of permafrost occurrence rather than the absolute permafrost distribution.

The model training process involves randomly selecting 70% of the samples as training samples, and the remaining 30% of the samples are used for the model validation (testing). The evaluations of model performance for both the training and testing processes are calculated separately. The independent model training and testing processes are expected to substantially reduce the uncertainties in the model predictions. The performance of the model was evaluated by calculating the area under the receiver operating characteristic (AUROC) curves (Hosmer et al., 2013; Rahman et al., 2019, 2021). The model results were also compared with the global permafrost zonation index (Gruber, 2012) for a quantitative comparison of the current permafrost probability distributions. A sensitivity analysis of the model conditioning factors (independent variables, i.e., elevation, near-surface air temperature and net radiation) is performed. Three different values for the relative decrease (RD) in the AUROC curve are calculated by

separately excluding one of the three conditioning factors and keeping the other two. Similarly, three different permafrost probability distributions were computed by separately excluding one of the three independent variables during sensitivity analysis. This process is supposed to reflect the dependency of the model on the independent variables. RD can be calculated as Eq. (2):

$$RD = \frac{AUC_{all} - AUC_i}{AUC_{all}} \times 100 \quad (2)$$

where AUC_{all} is the value of the AUROC curve obtained using all three independent variables and AUC_i is the value of the AUROC curve with the i^{th} independent variable excluded.

3. Results

3.1. Rock glacier inventory and distribution

Our rock glacier inventory of the Hunza Basin consists of a total of 616 rock glaciers with high certainty index scores, and these landforms cover an area of 194 km^2 (Table S5). We identified 227 intact debris rock glaciers, 42 relict debris rock glaciers, 223 intact talus rock glaciers, and 124 relict talus rock glaciers in the inventory. The spatial distribution of the categorized rock glaciers in the Hunza Basin are shown in Fig. 1c. The highest elevation of the root zones of the rock glaciers is ~5700 m a.s.l. The mean elevation of the rock glaciers in the catchment is 4568 m a.s.l., and ~ 76% of the rock glaciers are between 3900 and 4900 m a.s.l. The rock glaciers are concentrated in the northern Hunza Basin. The lowest elevation of the debris rock glaciers is ~2776 m a.s.l. in the upper Hunza Basin. About 93% of the rock glaciers are located within the Upper Hunza basin shown in Fig. 1c.

Rock glaciers are abundant in the catchment with 347 talus rock glaciers (56%) and 269 debris rock glaciers (44%). The majority of debris rock glaciers are originated from either small debris-covered glaciers or glacial moraines. Large rock glaciers are developed from debris rock glaciers, and the presence of abundant ice mixed with debris provides sufficient moisture for growth. We found a total of 26 rock glaciers with areas greater than 1 km^2, whereas 3 rock glaciers had areas greater than 2 km^2. The largest rock glacier covers an area of 2.90 km^2 with an elevation range of 3571 m a.s.l. to 5100 m a.s.l. Approximately 68 rock glaciers descend down to the valley floors and interact with rivers. The shorelines of former lakes are observed, and lacustrine deposits of sand and silt are observed along the former banks of the lakes. A few examples of the interactions of rock glaciers with river channels and surface features can be seen in Fig. S7. Further investigation is needed to quantify the formation, volume, and breaching of the rock glacier dams in the catchment.

3.2. Destabilized rock glacier and interaction with river channel

Detail analysis of the 68 destabilization rock glaciers, which interacted with river channels in the catchment is performed. About 35 rock glaciers with an area range between 0.012 and 1.54 km^2 are affected by destabilization and identified as being susceptible to blocking and obstructing river channels with evidences of previous rock glacier dams (Table S6). Some of these destabilized rock glaciers showed higher mean annual surface velocities (0.01–1.54 m a^{-1}) between 1973 and 2019. About 15 destabilized rock glaciers diverted the river channel and do not shown any significant evidences of rock glacier dam with lower velocities (0.05–0.67 m a^{-1}) and area range between 0.04 and 1.05 km^2. All of the analyzed 68 rock glacier showed surface disturbances, details of the destabilized features along with the mean surface velocity and rock glacier dam features are given in Table S6 and the location provided as shapefile in the supplement. All of these destabilized rock glaciers are located in the upper Hunza Basin. Some of these rock glaciers are formed by the combination of two or more tributary rock glaciers. The root zones of ice-fed rock glaciers and the foot zones of talus rock glaciers showed high velocities but not all of the destabilized rock glaciers followed the same high and low velocities at root zone and foot zone. Several factors can lead to destabilize the rock glacier such as thermal regime, geometry and mechanical causes (Delaloye et al., 2013; Ikeda et al., 2008).

Cracks and crevasses are the dominant features of the destabilized rock glaciers (~88%) in the catchment shown in Fig. 2 for the destabilized rock glacier (ID 503) which also interacted with river channel. Rock glacier (ID 503) is extended to 1.27 km^2 area with an elevation range between 4170 and 5150 m a.s.l., located in the northern part of the catchment. The destabilized rock glacier showed cluster of crakes and deep crevasses along the margins of the high and low velocity regions (Fig. 2a, b and c). It might be because of the variation in stresses due to acceleration and deacceleration of certain portion of the rock glacier. Surface topography over which the rock glacier (Fig. 2a-f) is developing also seems to be the major influencing factor for the rock glacier destabilization. The high velocities of certain areas within the rock glaciers can be attributed to the geometry. High concentrations of ice mixed with debris load can also lead to increase the rate of topo-climatic-driven creep (Buchli et al., 2017). Over the steep slopes rock glacier experienced maximum surface disturbances (1 and 2 in Fig. 2 highlighted by red circles) which favors the higher stresses and velocity variation. The high velocity regions are also located within the zero-degree isotherm zone for the months of May (4500 m a.s.l.) and June (5000 m a.s.l.). Foot zones of the majority of the analyzed destabilized rock glacier descent down to the valley floor over the transitional slope inclination from steep to gentle slope which favors the compressional flow structures (Fig. 2d). The rock glacier (ID 503) has obstructed the river flow at valley floor and rock glacier dam features can be seen in the Fig. 2a. Variation in the creep rate at the root zone of the destabilized rock glacier can potentially block the river flow.

3.3. Climate change trend analysis

We performed a trend analysis using the nonparametric Mann-Kendal test and Sen's slope to quantify the magnitude of the trend (Yue et al., 2002). Daily data for 1995–2019 are selected from 16 meteorological stations with 10 stations located above 3000 m a.s.l. as shown in Table S4 These high-elevation weather stations show a slightly increasing trend in the maximum temperature (T_{max}), except Khunjerab (4730 m a.s.l.) and Askoli (3015 m a.s.l.) stations showing a slightly negative trends of −0.28 °C a^{-1} and -0.27 °C a^{-1}, respectively ($P < 0.05$). Burzil (4239 m a.s.l.) and Deosi (4149 m a.s.l.) located in the eastern part of the Astore Basin show slightly increasing precipitation trends of 0.10 mm a^{-1} and 0.05 mm a^{-1}, respectively ($P < 0.05$). Detailed analysis of the maximum temperature (T_{max}), minimum temperature (T_{min}), and precipitation based on the three weather stations within the Hunza Basin (Khunjerab, Ziarat and Naltar, at 4730, 3668 and 2898 m a.s.l., respectively) are shown in Table S3.

The mean monthly temperatures are between −20.81 °C and 23.03 °C during January–July at the Khunjerab and Naltar stations. All three meteorological stations in the Hunza Basin show slightly decreasing trends in minimum and maximum temperatures of −0.2 °C a^{-1} and -0.04 °C a^{-1}, respectively, at 0.05 α during 1995–2019 ($P < 0.05$). We observed a slightly increasing temperature trend during January–April at all three stations (Figs. S1, S2 and S3). Both T_{max} and T_{min} have increasing trends during February. T_{min} during February significantly increased at all three stations at rates of 0.10 °C a^{-1} ($P < 0.1$), 0.13 °C a^{-1} ($P < 0.05$), and 0.07 °C a^{-1} ($P < 0.1$) at Khunjerab, Ziarat, and Naltar, respectively. Similarly, February precipitation shows slight increasing trends at Khunjerab and Ziarat at rates of 0.42 mm a^{-1} ($P < 0.01$) and 1.85 mm a^{-1} ($P < 0.05$), respectively (Table S3). Winter precipitation (November–December) significantly increases at Khunjerab and Ziarat. The mean monthly T_{max} decreases insignificantly during August and September at a range of rates from −0.01 °C a^{-1} to −0.08 °C a^{-1}.

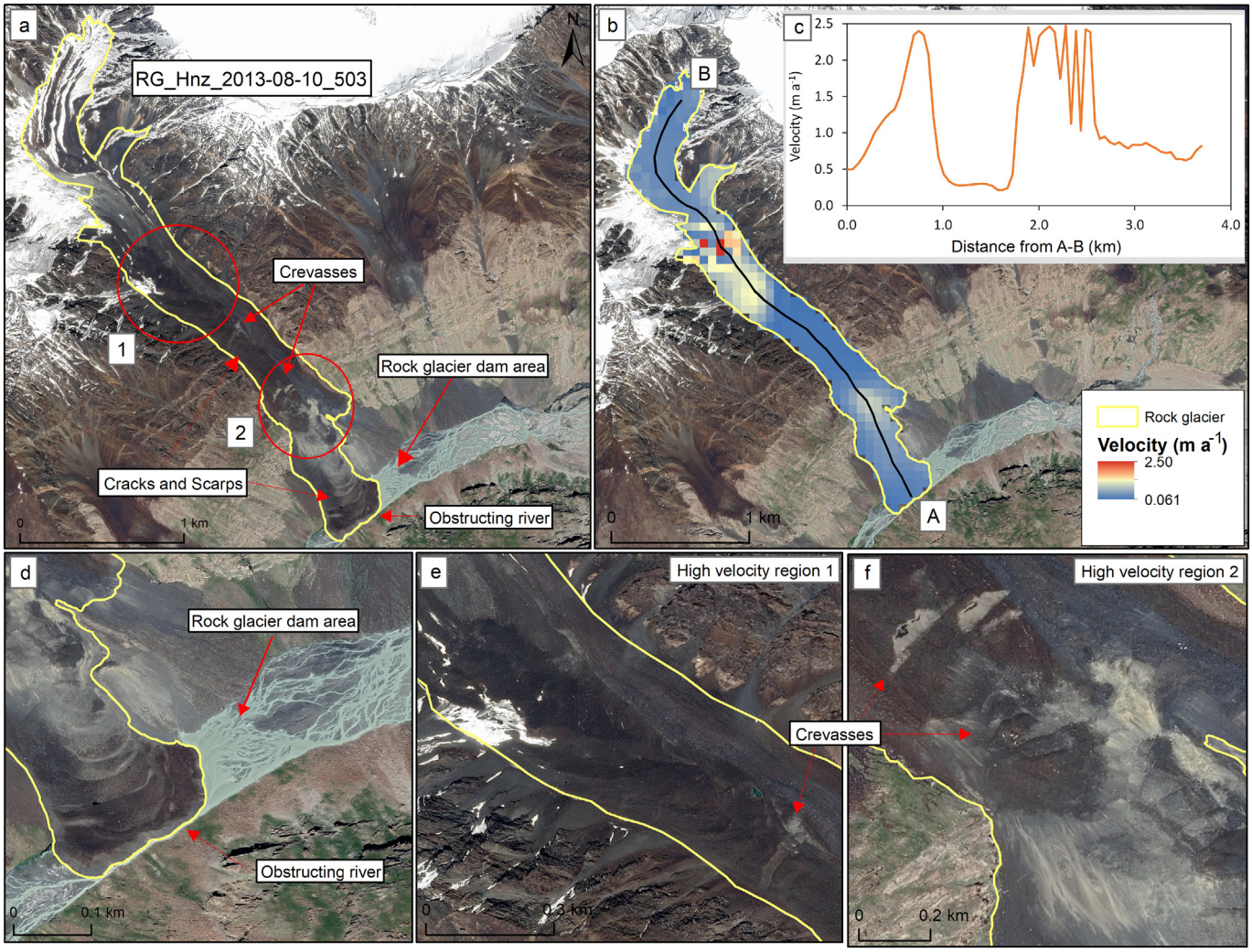

Fig. 2. (a) Google Earth map of one of the destabilized rock glaciers 503 along with the surface morphological indicators. (b) The mean annual velocity from 2016 to 2019. (c) Variations in surface velocity along the flow line A-B of rock glacier 503. (d) Destabilized rock glaciers obstructing a river channel and the rock glacier dam area is shown. (e) The region of high surface velocity (1 and 2) encircled in panel (a) is shown along with the destabilization surface features. (f) The location of the rock glacier in the Hunza Basin is highlighted by circle shown in this figure and details are given in an inventory in Table S4 and Table S5.

In addition, the number of wet days significantly increased by 3.94 days a^{-1} ($P < 0.01$), 4.91 days a^{-1} ($P < 0.001$), and 2.14 days a^{-1} ($P < 0.05$) at Khunjerab, Ziarat, and Naltar, respectively. The climate change trend analysis of the meteorological stations is presented in Figs. S1, S2 and S3.

3.3.1. Zero-degree (0 °C) isotherm

We estimated a zero-degree isotherm using meteorological datasets from Khunjerab, Ziarat and Naltar stations (Fig. S8) and found good agreement with the PZI ≥ 0.5. The zero-degree isotherm is the 0 °C altitude observed during 1995–2019. We obtained 3800 m a.s.l. as the mean annual zero-degree isotherm. The PZI ≥ 0.5 was observed at as low as 3525 m a.s.l. The minimum elevation of the zero-degree isotherm during January is ~1700 m a.s.l. and its maximum elevation is 5500 m a.s.l. during July. Previous studies used climate data from valley-based stations with shorter temporal extents (Archer, 2004) than the 1995–2019 period used in this study. Khan et al. (2015) estimated 5515 m a.s.l. as the maximum elevation of the zero-degree isotherm for the Hunza Basin using climate data from 1999 to 2002 combined with satellite images. Hewitt (2011) estimated between 4800 m a.s.l. and 5200 m a.s.l as the maximum elevation of the zero-degree isotherm, while Hasson et al. (2013) derived a zero-degree isotherm between 3400 m a.s.l. and 3500 m a.s.l. The mean monthly variation in the zero-degree isotherm is shown in Fig. S8.

3.4. Permafrost zonation index (PZI) and rock glacier distribution along the PZI

Based on the categorized rock glaciers (Table S5) and topo-climatic variables, we estimated the mean annual, summer (June–September) and the entire study period permafrost probability distribution during 1995–2019 (Fig. 3a, b). The probability value of PZI ≥ 0.5 agrees well with the zero-degree isotherm calculated using the in situ measured near-surface air temperatures from all three meteorological stations in the Hunza Basin. Therefore, a critical value of 0.5 on the model-generated PZI is chosen to discriminate between "permafrost presence" (PZI ≥ 0.5) and "permafrost absence" (PZI < 0.5), where the PZI ranges from 0.00–1.00. A probability threshold of PZI ≥ 0.5 is also adopted in a number of studies in other glaciated regions of the Himalayas (Baral et al., 2020; Haq and Baral, 2019). We generated a permafrost probability map with 30 m spatial resolution for the Hunza Basin. Approximately 85% of the catchment area lies within the mean annual permafrost probability zone of PZI ≥ 0.5. The minimum elevation of the permafrost probability zone of PZI values from 0.50–0.59 is 3525 m a.s.l. The maximum area (5153 km^2; 38%) of the PZI occurs between the PZI values of 0.80 to 0.89 within the elevation range from 4550 m a.s.l. to 5450 m a.s.l. The PZI values between 0.90 and 1.00 are predicted to be between the

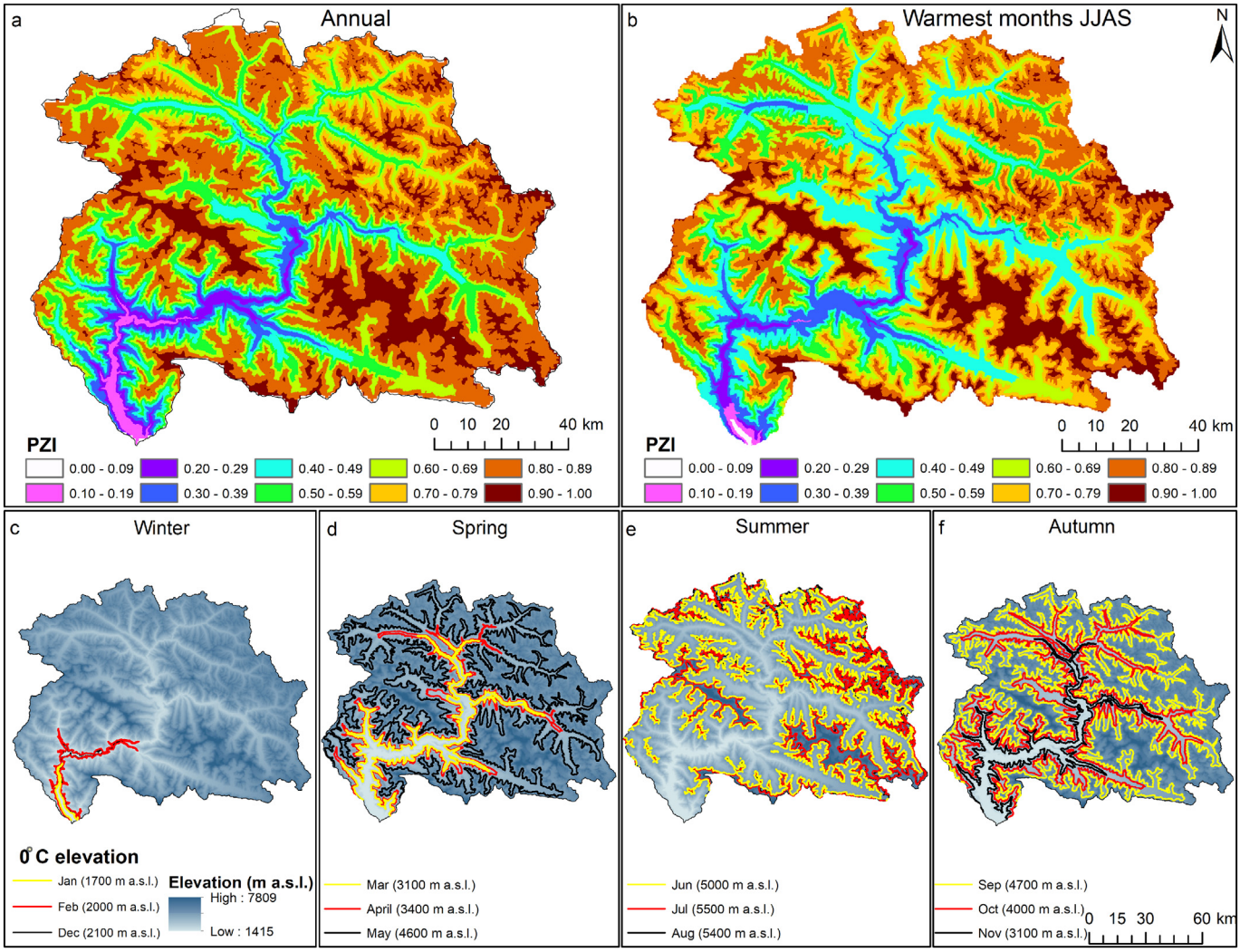

Fig. 3. Probability distribution of permafrost (a) on an annual basis and (b) for the warmest months of the year. (c-f) Annual variations in the zero-degree altitude on monthly and seasonal bases from 1995 to 2019 based on the in situ recorded mean monthly temperatures are shown for the representative months with elevation contour lines.

elevations of 5616 m a.s.l. to 7693 m a.s.l. covering an area of 1495 km^2 (11%). The altitudinal area distribution of the permafrost probability for each range of PZI values is shown in Fig. 4a. More than 70% of the entire study area lies above 4000 m a.s.l., which is mostly comprised of the upper Hunza Basin. The climate and geomorphological setting of the Hunza Basin provide sufficient ingredients and favorable conditions for the existence of permafrost above 4000 m a.s.l. as predicted by our model. A total of 76.2% of the area of rock glaciers is between 3900 m a.s.l. and 4865 m a.sl. Approximately 52% of both intact and relict rock glaciers lie within PZI ≥ 0.6, which starts from a minimum elevation of 4000 m a.s.l. Only a small quantity of rock glaciers are distributed in PZI ≥ 0.7. The distribution of the rock glacier area compared with the elevation and PZI is shown in Fig. 4b and 6c, respectively, and the number of intact and relict rock glaciers compared with the PZI is shown in Fig. 4d. A slight reduction in the permafrost probability distribution during the warmest months of the year is observed (Fig. 4b). The mean minimum elevation of PZI ≥ 0.5 is ~4500 m a.s.l. in summer.

The accuracy of the model-predicted permafrost probability distribution is determined by calculating the area under the receiver operating characteristic (AUROC) curves. For the cross-validation of our result, we calculated the AUROC over the global permafrost zonation index (Gruber, 2012) using our intact and relict rock glacier inventory from the Hunza Basin. AUROCs of 0.98 and 0.97 were obtained during model training and testing for the current modeled permafrost zonation index, respectively. AUROCs of 0.89 and 0.96 for model training and testing are estimated for the global permafrost zonation index, respectively, as shown in Fig. S4a-b. This indicates that the accuracy of the model's predictive capabilities strongly depends on the classification of the rock glaciers. Based on the sensitivity analysis of the model independent variables, elevation is the most sensitive and influencing predictor with a RD of 30%. The model performance is reduced by a RD of 28% by excluding net radiation followed by the temperature with a RD of 24%.

3.5. Landslides and hazards associated with variations in permafrost and rock glaciers

Changes in climate-induced permafrost freezing and thawing can enhance the mechanisms of slope failure. Permafrost creep can transport debris to the locations from where debris flows or landslides originate (Kääb, 2008). A detailed investigation of the Hassan-abad catchment, which is nested within the Hunza Basin, is performed to investigate permafrost-associated hazards. We identified two critical creeping slopes (i and ii) and a landslide, as shown in Fig. 5c, d. A series of images of the detaching of slope (i) and the landslide is presented in Figs. S6 and S7, respectively. The creeping slope (i) was detached at an elevation of 4000 m a.s.l. The detached slope (i) is located between the upper boundary of annual PZI values 0.50–0.59 and the lower boundary of annual PZI values 0.6–0.69. Annual and seasonal variations in freezing and thawing between PZI boundaries are expected to have

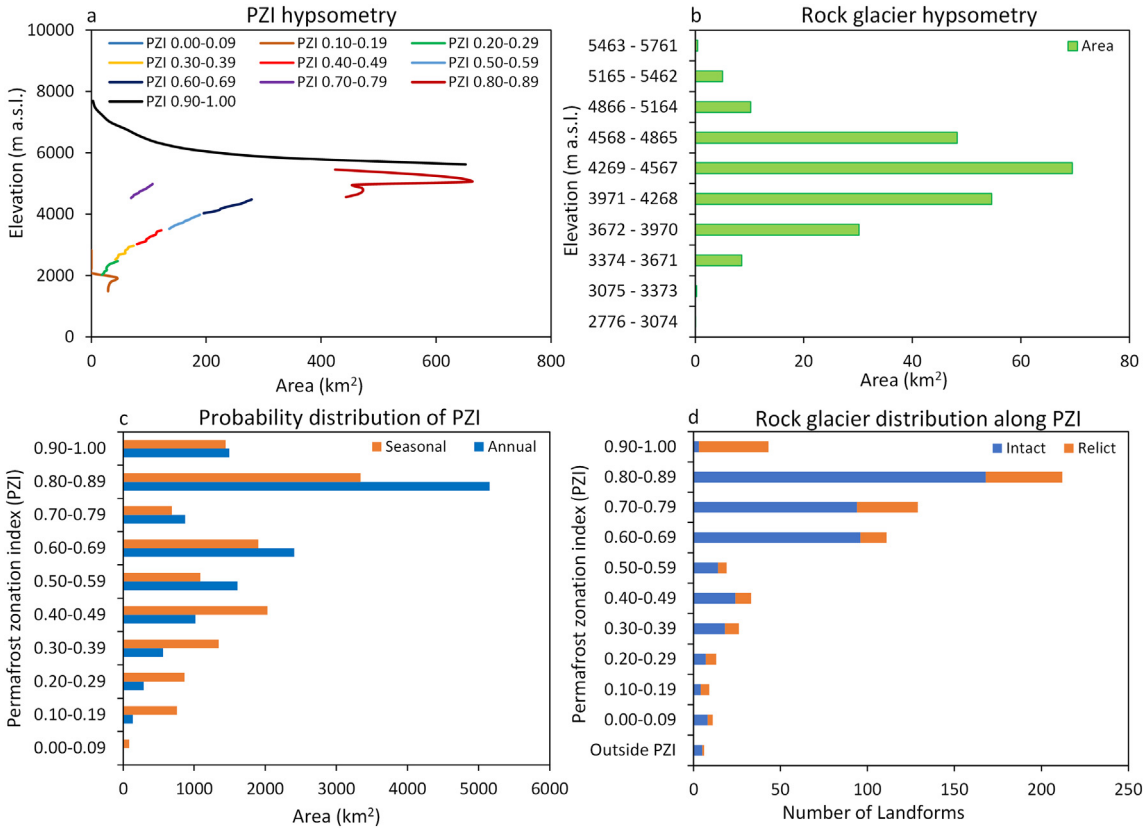

Fig. 4. (a) Altitudinal variations in the probability distribution of the permafrost zonation index (PZI). (c) Mean annual variation in area of each PZI from 1995 to 2019 and for the warmest months of the year. (b) The area distribution of rock glaciers along different altitude ranges in the Hunza Basin. (d) The distribution of intact and relict rock glaciers over PZI.

significant influences on slope destabilization in the catchment. The creeping slope (i) within the permafrost zone was detached in June 2017, and the sharp shift in temperatures during the transitional period between spring and early summer might have triggered the creep movement of the slope (Table S3). Subsequently, the creeping slope (i) continued to move until 2018 (Fig. S5f), and a significant amount of mass was transported down the slope. The landslide and failures of the creeping slopes (i and ii) can potentially block the downstream river with a high probability of water damming at the bottom of the narrow valley. The narrow valley was previously blocked by a major landslide during 5–25 July 2010, approximately 2.2 km away from the outlet of the Hassan-abad catchment (Fig. S6). The location and a series of images of the landslide are shown in Fig. S6a-g. The mean elevation of the landslide area is approximately 3500 m a.s.l., and the upper part of the landslide area overlapped with the lower limits of PZI values from 0.50–0.59. The initial landslide area was approximately 4.5 km^2, and the subsequent failure of mass extended the area up to 5 km^2. The landslide blocked the river several times, generated periodic floods and caused significant damage to the infrastructure at the outlet of the Hassan-abad catchment.

Some of the damage made by the periodic floods caused by the landslide at the outlet of the Hassan-abad catchment is presented in Fig. 6. The landslide area was also composed of summer fields and pasture lands. The failure of unstable material along the margins of the initial landslide increased the landslide area to 5 km^2. An old bridge was partially damaged during the flood caused by the initial landslide in 2010. A subsequent landslide blocked the river and caused a flood in 2012, which swept way an old bridge at the catchment outlet (Fig. 6a, h). Periodic floods over time have destroyed the water supply system composed of water tanks and irrigation channels adjacent to the outlet of the Hassan-abad catchment (Fig. 6e-g). Because of the damage from consecutive floods, a new bridge has been constructed north of the Hassan-abad catchment outlet (Fig. 6a, i and j). A hydropower plant located upstream of the Hassan-abad catchment outlet approximately 0.4 km away (Fig. 5a and 6a-d) was demolished by the flood during 2017–2018, as shown in Fig. 6b, c and d. Changes in the water course caused by periodic floods originating from the Shisper and Muchuhar glaciers have damaged the hydropower plant. No supraglacial lake or glacial ice dam lake was observed during this period. Climate data for the same flood period from the catchment did not show any anomalies in either temperature or precipitation. Subglacial or in-glacial lake outbursts could have poured excess water into river systems. The only part of the hydropower plant that is currently standing is a remnant of the lateral wall (Fig. 6d). The tops of the landslide and creeping slopes presented in Fig. 5 are demolished and currently unreachable; therefore, our team was not able to collect current ground information.

Periodic landslides and floods in the Hassan-abad catchment have displaced populations, and significant damage has been reported by the local administration. The populated village and settlements are only a kilometer away from the catchment outlet, as shown in Fig. 5a. The strategically important Karakoram Highway (KKH), which connects Pakistan and China through the China-Pakistan Economic Corridor (CPEC), is approximately 2.3 km away from the catchment outlet. Local sources have revealed that the upstream changes in the cryosphere are causing significant damage to the settlements and the KKH. The catchment is susceptible to cryospheric hazards and disasters because of the significant permafrost distribution and the potential obstruction of river channels by rock glaciers.

4. Discussion

We compiled the first systemic and complete inventory of rock glaciers in the Hunza Basin of the Karakoram region. Approximately 44% of the rock glaciers in the Hunza Basin are identified as originating from debris and 88% of the rock glaciers are confined within upper Hunza basin. Few studies have been conducted in the Karakoram to assess

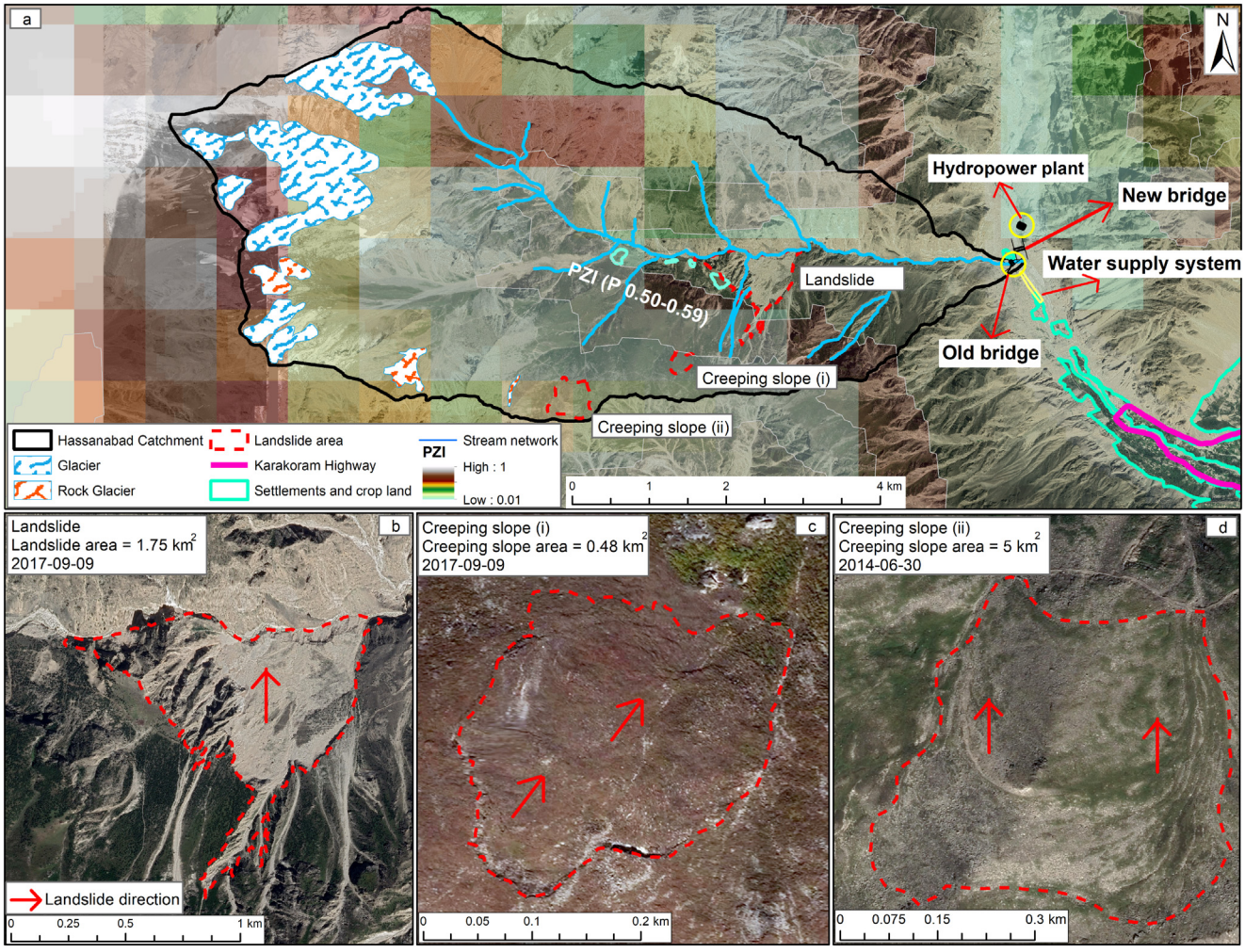

Fig. 5. (a) The two critical creeping slopes (i and ii) and landslide area is located with the help of red dotted line in Hassan-abad catchment overlapped along with the annul PZI. Gray contour boundary shows the PZI (P 0.50-0.59) and the infrastructure damaged by the periodic floods and debris flow are highlighted at the catchments outlet in panel (a). Major landslide occurred between July-November 2010 (b) and the creeping slope detached in June 2017 located between the boundary of annual PZI (P 0.50-0.59) and (0.6-0.69) (c). Large area of a creeping slope (ii) located within the PZI (P 0.80-0.89) is presented in panel (d) red arrows showing the direction of slope failure and creep movement. (For interpretation of the references to color in this figure legend, the reader is referred to the online version of this chapter.)

the characteristics of rock glaciers and the occurrence of permafrost in the region. Jones et al. (2021) estimated about 7240 number of rock glacier for western Himalayas and are the critical components of the Himalayan hydrology with a relative importance of 1:25 versus glaciers. Owen and England (1998) investigated the selected rock glaciers in the Himalaya and Karakoram mountains of northern Pakistan and India and suggested that most of the rock glaciers in the region are ice-cored moraines derived from post-Little Ice Age glacier retreat. Rock glaciers in the Karakoram region are restricted within the particular climate envelope where annual precipitation is less than 1000 mm located above 4000 m a.s.l. and some descent down to valley floor (Owen and England, 1998). Bolch and Gorbunov (2014) hypothesized the intensive weathering and rock avalanches are the key drivers of the expansion of large rock glaciers in the Tien Shan. We found that abundant high-altitude moisture in the root zone and debris from glacial moraines, glaciers and surrounding rock slopes are the key features that account for the growth of rock glacier areas.

We observed, majority of the destabilized rock glaciers which interacted with river channel are comparatively large in size and can be closely related around the zero-degree isotherm. Crakes and crevasses are the dominant features of the destabilized rock glacier in the upper Hunza Basin with mean annual surface velocity range between 0.04 and 1.54 m a^{-1}. About 35 destabilized rock glaciers obstructed the river channel at valley floor, changes in the creep rate of these rock glacier can potentially block the river channel. The formation of rock glacier dams in the Karakoram region has also been reported (Blöthe et al., 2019). Blöthe et al. (2019) documented 5 rock glacier dams with an area of 142.4 km^2 that existed in the Karakoram region during 2019 and the breach of 11 former dams. Whereas, we found one rock glacier dam in the upper Hunza Basin; 35 of the rock glaciers can potentially form rock glacier dams, and 68 have interacted with river channels. It is evident that changes in the climatic conditions could influence the rock glacier destabilization as the strain rate increases proportionally with increase in melt water anticipated by increase in temperature (Arenson and Springman, 2011). Seasonal changes in the creep rate of the rock glacier is very likely controlled by hydrological processes (Buchli et al., 2017; Ikeda et al., 2008). Majority of the rock glaciers show high velocities at middle part and root zones, and the foot zones of the destabilized rock glaciers near the valley floor are generally stable, except for those of a few rock glaciers. High velocities in the root and foot zones of debris rock glaciers and talus rock glaciers can be attributed to high concentrations of ice mixed with debris. We found slightly increasing surface velocity of the rock glaciers in recent decades compared to the 1970s. Similarly, Kääb et al. (2020) found two to three fold increases in decadal surface velocities since the 1950s in the Ile Alatau and Kungöy Ala-Too mountain ranges.

The permafrost distribution cannot be visually identified; therefore, we adopted an indirect approach using the categorized rock glacier

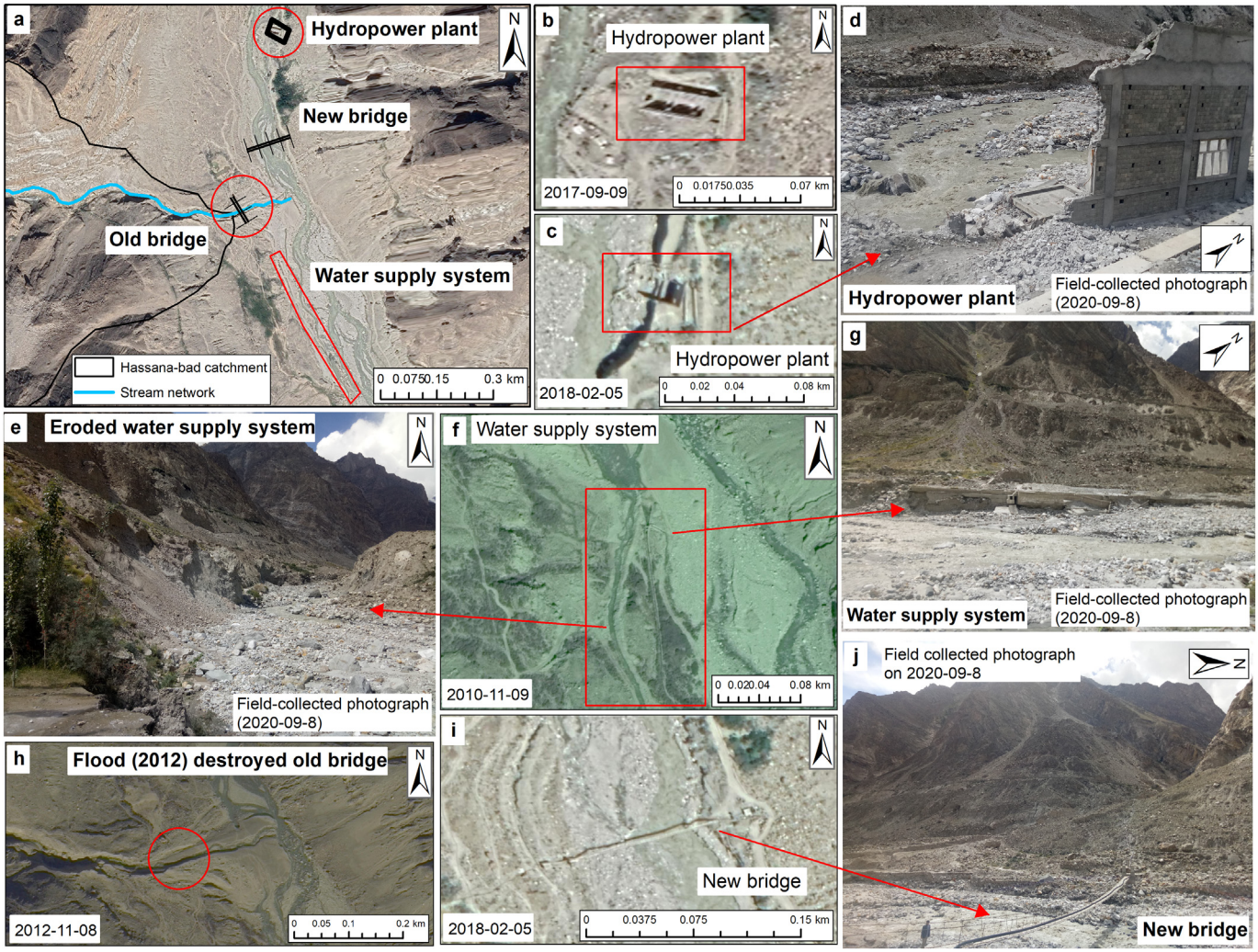

Fig. 6. Damage to infrastructure caused by cryospheric events that mostly originated from landslides, debris flows and glacial lake outburst floods are shown here by combining a series of Google Earth images with the field-collected photographs. (a) Base map at the outlet of the Hassan-abad catchment with major infrastructure destroyed by floods and debris flow located in the red circles and rectangular box. (b, c, d) A flood during 2018-2019 demolished the hydropower plant, and only the sidewall of the hydropower plant is standing. (e, f, g) Water supply system destroyed during the flood of 2010 and 2012, (h) which originated from the major land slide (i). Old bridge (a) also washed away during the flood of 2012 (h). Google Earth image and filed collected photograph of new constructed bridge in 2018 is presented in (i, and j), respectively. (For interpretation of the references to color in this figure legend, the reader is referred to the online version of this chapter.)

inventory along with topo-climatic predictors to determine the likelihood of permafrost existence. Near-surface air temperature is a significant and sensitive predictor of the presence or absence of permafrost. Freezing and thawing of the permafrost layer are closely linked with variations in surface temperature. The use of in-situ measured surface temperature is recommended to assess the permafrost distribution and depth (Baral et al., 2020; Gruber, 2012; Nicolsky et al., 2009). Due to the lack of ground observations of surface temperature, we relied on the long-term measured near-surface air temperature from 1995 to 2019. The long-term near-surface temperature (2 m) in-situ measurements along with the other climate variables and categorized rock glacier inventory is expected to reduce uncertainties in the estimation of permafrost probability distribution. Our permafrost distribution results of PZI ≥ 0.5 in the Hunza Basin suggest that permafrost is more likely to occur above 3525 m a.s.l. The permafrost probability distribution of PZI 0.80–0.89 hosts the majority of the PZI area (38%) between 4550 m a.s.l. and 5450 m a.s.l. Our results agree with the findings of Gruber (2012). The modeled occurrence of permafrost probability with PZI ≥ 0.5 agrees well with the mean annual zero-degree isotherm (~3800 m a.s.l.) during 1995–2019. Our estimated permafrost probability distribution results are also comparable with the global permafrost zonation by Gruber (2012). The slight differences in the obtained zero-degree isotherms are probably due to the use of various datasets and the different temporal and spatial extents of the climate datasets compared to previous studies (Kääb et al., 2012; Scherler et al., 2011).

Detailed investigations of creeping slopes and landslides with PZI ≥ 0.5 in the Hassan-abad catchment are closely linked with variations in the freezing and thawing of permafrost. Deposits from landslides and slope failures at the narrow valley floor blocked rivers and generated periodic floods that damaged infrastructure further downstream. Despite the potential hazardous consequences on infrastructure and settlements, rock glaciers and permafrost hazards are rarely studied in the region. However, glacial lake outburst floods (GLOFs) in the Hunza Basin are well documented. Iturrizaga (2005), Bazai et al. (2021) and Hewitt (1982) presented catastrophic GLOFs during the last century in the upper Hunza valleys with devastating impacts on infrastructure and population. The present study provides the preliminary results regarding the potential consequences of destabilized rock glacier interaction with river channels and permafrost variation.

Previous climate change trend analyses in the upper Indus Basin were primarily derived from the valley-based low-elevation meteorological stations focusing on macroscale variations (Akhtar et al., 2008; Ali et al., 2019). Our detailed microscale investigation of the in situ meteorological datasets shows a significant increasing temperature trend

during winter months, which can have drastic consequences on the rock glacier dynamics, permafrost and land stability, and rock glacier destabilization in the region. Unlike in the central and eastern Himalayas, the cryospheric response in the Karakoram region is more sensitive to changes in temperature than precipitation, as reported by Hassan et al. (2017) and Shrestha et al. (2015). An increase in winter temperature can alter cryospheric mass budgets by changing the form of precipitation from solid to liquid. The increase in temperature warms the surrounding atmosphere, potentially accelerates the melt rates in spring and early summer. Various studies have observed and projected warming climate trends in the HKH region (Farinotti et al., 2009; Forsythe et al., 2017; Hassan et al., 2017; Khadka et al., 2020; Lutz et al., 2016), which can possibly destabilize the frozen slope induced by variations in the extents of permafrost and rock glaciers. Variations in permafrost creep and rock glaciers can have serious consequences for geohazards in the region. Rock glacier destabilization and their interaction with river channels present threats to the local population and infrastructure.

4.1. Limitations and mitigations

We developed the rock glacier inventory for the entire Hunza Basin. Snow and cloud cover can introduce uncertainties in the rock glacier inventory. However, the use of high-resolution Google Earth and Planet images with the temporal coverage (2000–2019) in this study can significantly reduce the uncertainties in the rock glacier inventory. Because of the snow, shadow and cloud covers, some of the delineated landforms (45 polygons) are not included in the rock glacier inventory. The paleo-glacial deposits that originated from the periodic advances and retreats of glaciers can appear as similar land features to rock glaciers (Zhu et al., 2019). Such features that appear identical but are unconformable to rock glaciers are digitized for records and not included in further analysis. Visual interpretation of rock glacier boundaries can also introduce uncertainties to some extent. The digitization of rock glaciers based on morphological evidence following standards established in previous studies (Barsch, 1996; Jones et al., 2017; Scotti et al., 2013) has improved the ability to truly define the boundaries of rock glaciers. The certainty index has greatly improved the quality of the rock glacier inventory. The certainty index (Jones et al., 2017; Jones et al., 2021) helped to quantify the boundary of each digitized rock glacier. Analysis of the cloud/snow/shadow cover rock glaciers using Planet images improved to precisely delineate the rock glacier boundaries. We used a statistical approach to model the permafrost probability distribution. Physically based energy balance modeling of ground observation to access the distribution of permafrost could also provide more detailed information (Nicolsky et al., 2009). The accuracy of permafrost probability distribution modeling has been greatly improved by using the entire categorized rock glacier inventory. Previous studies have argued that remote sensing and model-derived gridded meteorological datasets are responsible for introducing uncertainties (Baral et al., 2020; Gruber, 2012). Processing the fine-resolution band with the minimum cloud and snow cover Landsat images enhanced the quantitative accuracy. Despite few limitations, these results are the baseline to improve our understanding of the least observed cryosphere components and associated hazards in the Karakoram.

5. Conclusion

To the best of our knowledge, we present the first complete systematic rock glacier inventory and permafrost probability distribution in the Hunza Basin, Karakoram. We identified 616 rock glaciers covering an area of 194 km^2 at a very high resolution (0.24 m), and the majority of these landforms (76%) are confined between 3900 and 4900 m a.s.l. The observed meteorological datasets and post-categorized rock glacier inventory are anticipated to advance the representation of the permafrost probability distribution. The model-predicted occurrence of PZI ≥ 0.5 is likely above 3525 m a.s.l. with a maximum area (38%) confined within the PZI from 0.80–0.89. The mean monthly zero-degree isotherm is approximately 3800 m a.s.l., which matches the model-predicted mean annual PZI well. The surface velocities of rock glaciers have increased slightly in the most recent decade compared to the 1970s. Sixty-eight destabilized rock glaciers reached the valley floor, and 35 rock glaciers are identified as susceptible to blocking/obstructing river channels. Abundant moisture supply from the upstream ice and extensive sources of debris load are possible reasons for their descents to the valley floor below the permafrost occurrence zone. The root zones of these destabilized rock glaciers at the valley floor are mostly stable with velocities less than 0.5 m a^{-1}. Foot zone of about 15 destabilized rock glaciers at valley floor diverted the river channel but did not form the rock glacier dam rock. Mentoring the variation in creep rate of these destabilized rock glaciers could provide a valuable information for disaster risk reduction and mitigating potential associated hazards.

Climate data from the catchment show a warming trend during winter months with statistically significant increase in the month February. An increase in winter temperature could induce large fluctuations in the extents of permafrost and rock glacier destabilization with devastating consequences, leading to landscape transformation. Winter precipitation also increases at the higher elevations of the catchment. The number of wet days slightly increases during summer months. Changes in the climatic conditions of the Karakoram region can have serious impacts on infrastructure and settlements. Assessments of landslides, creeping slopes, and periodic floods in the Hassan-abad catchment have fundamentally enriched our perception of land stability and floods associated with permafrost variations and rock glacier destabilization. Landslides originating from the lower boundary of PZI ≥ 0.5 can be attributed to climate variation. The subsequent blockage of streams in narrow valley floods has resulted in a number of consequential floods causing significant damage to the infrastructure and population. Failure of the creeping slopes can potentially lead to repeat flooding events in the catchment. Despite the ambiguous hydrological significance and resilience of rock glaciers and permafrost, a better understanding of these cryospheric components is of the utmost importance.

Supplementary data to this article can be found online at https://doi.org/10.1016/j.scitotenv.2021.146833.

CRediT authorship contribution statement

JH conceptualized and designed this study, performed simulations, analyzed and visualized the results, and completed the manuscript; XC and SM helped with result analysis, manuscript writing and editing, and improved the quality of research; NAB helped with the revision, result analysis and editing of the manuscript and improved the quality of the research.

Declaration of competing interest

The authors declare that the research was conducted in the absence of any commercial or financial relationships that could be construed as a potential conflict of interest. The authors declare that they have no conflicts of interest.

Acknowledgement

We thank the reviewer Alessandro Cicoira and one anonymous reviewer and the scientific editor Elena Paoletti for providing insightful comments on the research, which improved the quality of our research. We express our sincere gratitude to the Institute of Mountain Hazards and Environment-Chinese Academy of Sciences (IMHE-CAS) and the University of Chinese Academy of Sciences. This research work is a part of PhD research supported by the Chinese Government Fellowship program for Doctoral research. This work was supported by the Cryosphere Initiative of the International Centre for Integrated

Mountain Development (ICIMOD), Funded by Norway and by core funds of the ICIMOD contributed by the governments of Afghanistan, Australia, Austria, Bangladesh, Bhutan, China, India, Myanmar, Nepal, Norway, Pakistan, Sweden, and Switzerland. We are thankful to the Pakistan Meteorological Department (PMD) and the Pakistan Glacier Monitoring Research Centre-Water and Power Development Authority (GMRC-WAPDA) for collecting and providing the hydrometeorological data. We acknowledge the help received from Mr. Mazaffar Ali and Sajid Ali for the field work. We are grateful to the Planet's Education and Research Program and United States Geological Survey for providing the satellite imagery. We are thankful to COSI-Corr team for developing and making the tool available for research.

Funding

This research work is funded by The Second Tibetan Plateau Scientific Expedition and Research Program (STEP) (Grant No. 2019QZKK0904). And the study is also supported by the Comprehensive Investigation and Assessment of Natural Hazards in China-Pakistan Economic Corridor (Grant No. 2018FY100500).

References

Akhtar, M., Ahmad, N., Booij, M.J., 2008. The impact of climate change on the water resources of Hindukush–Karakorum–Himalaya region under different glacier coverage scenarios. J. Hydrol. 355 (1–4), 148–163. https://doi.org/10.1016/j.jhydrol.2008.03.015.

Ali, S., Shafqat, M., Eqani, S., Shah, S.T.A., 2019. Trends of climate change in the upper Indus basin region. Pakistan: implications for cryosphere. Environmental Monitoring and Assessment 191. https://doi.org/10.1007/s10661-018-7184-3.

Allen, S., Fiddes, J., Linsbauer, A., Randhawa, S., Saklani, B. and Salzmann, N., 2016. Permafrost studies in Kullu district, Himachal Pradesh. Current Science, 111: 550-553. doi: 10.18520/cs/v111/i3/550-553.

Anderson, R.S., Anderson, L.S., Armstrong, W.H., Rossi, M.W., Crump, S.E., 2018. Glaciation of alpine valleys: the glacier – debris-covered glacier – rock glacier continuum. Geomorphology 311, 127–142. https://doi.org/10.1016/j.geomorph.2018.03.015.

Archer, D., 2004. Hydrological implications of spatial and altitudinal variation in temperature in the upper Indus basin. Nord. Hydrol. 35. https://doi.org/10.2166/nh.2004.0015.

Arenson, L., Springman, S., 2011. Mathematical descriptions for the behaviour of ice-rich frozen soils at temperatures close to 0 °C. Can. Geotech. J. 42, 431–442. https://doi.org/10.1139/t04-109.

Ayoub, F., Leprince, S., Avouac, J.-P., 2009. Co-registration and correlation of aerial photographs for ground deformation measurements. ISPRS J. Photogramm. Remote Sens. 64 (6), 551–560. https://doi.org/10.1016/j.isprsjprs.2009.03.005.

Azam, M.F., Wagnon, P., Berthier, E., Vincent, C., Fujita, K., Kargel, J.S., 2018. Review of the status and mass changes of Himalayan-Karakoram glaciers. J. Glaciol. 64 (243), 61–74. https://doi.org/10.1017/jog.2017.86.

Azócar, G.F., Brenning, A., Bodin, X., 2017. Permafrost distribution modelling in the semi-arid Chilean Andes. Cryosphere 11 (2), 877–890. https://doi.org/10.5194/tc-11-877-2017.

Baral, P., Haq, M.A., Yaragal, S., 2020. Assessment of rock glaciers and permafrost distribution in Uttarakhand, India. Permafr. Periglac. Process. 31 (1), 31–56. https://doi.org/10.1002/ppp.2008.

Barsch, D., 1996. Rock-glaciers. Indicators for the Present and Former Geoecology in High Mountain Environments https://doi.org/10.2307/3060377.

Bazai, N.A., et al., 2021. Increasing glacial lake outburst flood hazard in response to surge glaciers in the Karakoram. Earth Sci. Rev. 212, 103432. https://doi.org/10.1016/j.earscirev.2020.103432 (In this issue).

Beniston, M., Farinotti, D., Stoffel, M., Andreassen, L.M., Coppola, E., Eckert, N., Fantini, A., Giacona, F., Hauck, C., Huss, M., Huwald, H., Lehning, M., López-Moreno, J.I., Magnusson, J., Marty, C., Morán-Tejéda, E., Morin, S., Naaim, M., Provenzale, A., Rabatel, A., Six, D., Stötter, J., Strasser, U., Terzago, S., Vincent, C., 2018. The European mountain cryosphere: a review of its current state, trends, and future challenges. Cryosphere 12 (2), 759–794. https://doi.org/10.5194/tc-12-759-2018.

Berthier, E., Brun, F., 2019. Karakoram geodetic glacier mass balances between 2008 and 2016: persistence of the anomaly and influence of a large rock avalanche on Siachen Glacier. J. Glaciol. 65 (251), 494–507. https://doi.org/10.1017/jog.2019.32.

Blöthe, J.H., Rosenwinkel, S., Höser, T., Korup, O., 2019. Rock-glacier dams in high Asia. Earth Surf. Process. Landf. 44 (3), 808–824. https://doi.org/10.1002/esp.4532.

Bocchiola, D., Soncini, A., 2019. Water Resources Modeling and Prospective Evaluation in the Indus River Under Present and Prospective Climate Change, Indus River Basin. Elsevier, pp., 17–56 https://doi.org/10.1016/B978-0-12-812782-7.00002-3.

Boeckli, L., Brenning, A., Gruber, S. and Noetzli, J., 2012. A statistical approach to modelling permafrost distribution in the European Alps or similar mountain ranges. The Cryosphere, Volume 6, Issue 1, 2012, pp.125–140, 6: 125–140. doi:https://doi.org/10.5194/tc-6-125-2012.

Bolch, T., Gorbunov, A.P., 2014. Characteristics and origin of rock glaciers in northern Tien Shan (Kazakhstan/Kyrgyzstan). Permafr. Periglac. Process. 25 (4), 320–332. https://doi.org/10.1002/ppp.1825.

Bolch, T., Kulkarni, A., Kääb, A., Huggel, C., Paul, F., Cogley, J.G., Frey, H., Kargel, J.S., Fujita, K., Scheel, M., 2012. The state and fate of Himalayan glaciers. Science 336 (6079), 310–314. https://doi.org/10.1126/science.1215828.

Brardinoni, F., Scotti, R., Sailer, R., Mair, V., 2019. Evaluating sources of uncertainty and variability in rock glacier inventories. Earth Surf. Process. Landf. 44. https://doi.org/10.1002/esp.4674.

Buchli, T., Kos, A., Limpach, P., Merz, K., Zhou, X., Springman, S., 2017. Kinematic investigations on the Furggwanghorn Rock Glacier, Switzerland. Permafr. Periglac. Process. 2018, 1–18. https://doi.org/10.1002/ppp.1968.

Consortium, R., 2017. Randolph glacier inventory—a dataset of global glacier outlines: version 6.0. Global Land Ice Measurements from Space, Colorado, USA, Tech. Rep, https://doi.org/10.3189/2014JoG13J176. doi:https://doi.org/10.3189/2014JoG13J176.

Copland, L., Pope, S., Bishop, M.P., Shroder, J.F., Clendon, P., Bush, A., Kamp, U., Bae Seong, Y., Owen, L.A., 2009. Glacier velocities across the central Karakoram. Ann. Glaciol. 50 (52), 41–49. https://doi.org/10.3189/172756409789624229.

Delaloye, R., Perruchoud, E., Avian, M., Kaufmann, V., Bodin, X., Hausmann, H., Ikeda, A., Kääb, A., Kellerer-Pirklbauer, A., Krainer, K., Lambiel, C., Mihajlovic, D., Staub, B., Gärtner-Roer, I. and Thibert, E., 2008. Recent Interannual Variations of Rock Glacier Creep in the European Alps. 9th International Conference on Permafrost, https://doi.org/10.5167/uzh-7031. doi:https://doi.org/10.5167/uzh-7031.

Delaloye, R., Morard, S., Barboux, C., Abbet, D., Gruber, V., Riedo, M., Gachet, S., 2013. Rapidly moving rock glaciers in Mattertal. Mattertal - Ein Tal in Bewegung 21–31.

Delaloye, R., Barboux, C., Bodin, X., Brenning, A., Lea, H., Hu, Y., Ikeda, A., 2018. Rock Glacier Inventories and Kinematics: A New IPA Action Group, 5 Th European Conference on Permafrost. Edytem, Chamonix, France.

Elizabeth Martin, H., Whalley, W.B., 1987. Rock glaciers:part 1: rock glacier morphology: classification and distribution. Progress in Physical Geography: Earth and Environment 11 (2), 260–282. https://doi.org/10.1177/030913338701100205.

Farinotti, D., Huss, M., Bauder, A., Funk, M., Truffer, M., 2009. A method to estimate the ice volume and ice-thickness distribution of alpine glaciers. J. Glaciol. 55 (191), 422–430. https://doi.org/10.3189/002214309788816759.

Farinotti, D., Huss, M., Fürst, J.J., Landmann, J., Machguth, H., Maussion, F., Pandit, A., 2019. A consensus estimate for the ice thickness distribution of all glaciers on Earth. Nat. Geosci. 12 (3), 168.

Forsythe, N., Fowler, H.J., Li, X.-F., Blenkinsop, S., Pritchard, D., 2017. Karakoram temperature and glacial melt driven by regional atmospheric circulation variability. Nat. Clim. Chang. 7 (9), 664–670. https://doi.org/10.1038/nclimate3361.

Gruber, S., 2012. Derivation and analysis of a high-resolution estimate of global permafrost zonation. Cryosphere 6. https://doi.org/10.5194/tc-6-221-2012.

Gruber, S., Fleiner, R., Guegan, E., Panday, P., Schmid, M.O., Stumm, D., Wester, P., Zhang, Y., Zhao, L., 2017. Review article: inferring permafrost and permafrost thaw in the mountains of the Hindu Kush Himalaya region. Cryosphere 11 (1), 81–99. https://doi.org/10.5194/tc-11-81-2017.

Haeberli, W., 1985. Creep of mountain permafrost: internal structure and flow of alpine rock glaciersmitteilungen Der versuchsanstalt fur wasserbau. Hydrologie und Glaziologie an Der ETH Zurich 77, 5–142.

Haq, M.A., Baral, P., 2019. Study of permafrost distribution in Sikkim Himalayas using Sentinel-2 satellite images and logistic regression modelling. Geomorphology 333, 123–136. https://doi.org/10.1016/j.geomorph.2019.02.024.

Harrison, S., 2009. Climate sensitivity: implications for the response of geomorphological systems to future climate change. Geol. Soc. Lond., Spec. Publ. 320, 257–265. https://doi.org/10.1144/SP320.16.

Hassan, J., Kayastha, R.B., Shrestha, A., Bano, I., Ali, S.H., Magsi, H.Z., 2017. Predictions of future hydrological conditions and contribution of snow and ice melt in total discharge of Shigar River Basin in Central Karakoram, Pakistan. Sciences in Cold and Arid Regions 9 (6), 0511–0524. https://doi.org/10.3724/SP.J.1226.2017.00511.

Hasson, S.u., Lucarini, V., Khan, M.R., Petitta, M., Bolch, T., Gioli, G., 2013. Early 21st century climatology of snow cover for the western river basins of the Indus River System. Hydrol. Earth Syst. Sci. Discuss. 10, 13145–13190. https://doi.org/10.5194/hessd-10-13145-2013.

Hewitt, K., 1982. Natural Dams and Outburst Floods of the Karakoram Himalaya. IAHS-AISH Publication.

Hewitt, K., 2011. Glacier change, concentration, and elevation effects in the Karakoram Himalaya, Upper Indus Basin. Mt. Res. Dev. 31, 188–200. https://doi.org/10.1659/MRD-JOURNAL-D-11-00020.1.

Hewitt, K., 2014. Glaciers of the Karakoram Himalaya, https://doi.org/10.1007/978-94-007-6311-1, 429–436 pp.

Hewitt, K., Wake, C.P., Young, G., David, C., 1989. Hydrological investigations at Biafo Glacier, Karakoram Range, Himalaya; an important source of water for the Indus River. Ann. Glaciol. 13, 103–108. https://doi.org/10.3189/s0260305500007710.

Hosmer, W. David, Stanley Lemeshow, Rodney X. Sturdivant, 2013. Applied Logistic Regression. John Wiley & Sons, Inc, 3rd Edition: 173–182. doi:https://doi.org/10.1002/9781118548387

Huss, M., Hock, R., 2015. A new model for global glacier change and sea-level rise. Front. Earth Sci. 3, 54.

Huss, M., Hock, R., 2018. Global-scale hydrological response to future glacier mass loss. Nat. Clim. Chang. 8 (2), 135.

Ikeda, A., Matsuoka, N., Kääb, A., 2008. Fast deformation of perennially frozen debris in a warm rock glacier in the Swiss Alps: an effect of liquid water. J. Geophys. Res. 113. https://doi.org/10.1029/2007JF000859.

Immerzeel, W., Wanders, N., Lutz, A., Shea, J., Bierkens, M., 2015. Reconciling high-altitude precipitation in the upper Indus basin with glacier mass balances and runoff. Hydrol. Earth Syst. Sci. 19 (11), 4673–4687. https://doi.org/10.5194/hess-19-4673-2015.

Ipcc, McDowell, G., Barr, I., 2019. 'High Mountain Areas' chapter - IPCC Special Report on the Oceans and Cryosphere in a Changing Climate (SROCC).
Iturrizaga, L., 2005. New observations on present and prehistorical glacier-dammed lakes in the Shimshal valley (Karakoram Mountains). J. Asian Earth Sci. 25 (4), 545–555. https://doi.org/10.1016/j.jseaes.2004.04.011.
Jin, H., Li, S., Cheng, G., Shaoling, W., Li, X., 2000. Permafrost and climatic change in China. Glob. Planet. Chang. 26 (4), 387–404. https://doi.org/10.1016/S0921-8181(00)00051-5.
Jones, D., Harrison, S., Anderson, K., Selley, H., Wood, J., Betts, R.A., 2017. The distribution and hydrological significance of rock glaciers in the Nepalese Himalaya. Glob. Planet. Chang. 160. https://doi.org/10.1016/j.gloplacha.2017.11.005.
Jones, D.B., Harrison, S., Anderson, K., 2019a. Mountain glacier-to-rock glacier transition. Glob. Planet. Chang. 181, 102999. https://doi.org/10.1016/j.gloplacha.2019.102999.
Jones, D.B., Harrison, S., Anderson, K., Whalley, W.B., 2019b. Rock glaciers and mountain hydrology: a review. Earth Sci. Rev. 193, 66–90. https://doi.org/10.1016/j.earscirev.2019.04.001.
Jones, D.B., Harrison, S., Anderson, K., Shannon, S. and Betts, R.A., 2021. Rock glaciers represent hidden water stores in the Himalaya. Science of the Total Environment, https://doi.org/10.1016/j.scitotenv.2021.145368: 145368. doi:https://doi.org/10.1016/j.scitotenv.2021.145368.
Kääb, A., 2008. Remote sensing of permafrost-related problems and hazards. Permafr. Periglac. Process. 19 (2), 107–136. https://doi.org/10.1002/ppp.619.
Kääb, A. and Weber, M., 2004. Development of transverse ridges on rock glaciers: field measurements and laboratory experiments. Permafrost and Periglacial Processes, 15(4): 379-391. doi:doi.org/10.1002/ppp.506
Kääb, A., Kaufmann, V., Ladstädter, R., Eiken, T., 2003. Rock glacier dynamics: implications from high-resolution measurements of surface velocity fields. Permafrost 501–506.
Kääb, A., Berthier, E., Nuth, C., Gardelle, J., Arnaud, Y., 2012. Contrasting patterns of early twenty-first-century glacier mass change in the Himalayas. Nature 488 (7412), 495. https://doi.org/10.1038/nature11324.
Kääb, A., Strozzi, T., Bolch, T., Caduff, R., Trefall, H., Stoffel, M., Kokarev, A., 2020. Inventory, motion and acceleration of rock glaciers in Ile Alatau and Kungöy Ala-Too, northern Tien Shan, since the 1950s. The Cryosphere Discuss. 2020, 1–37. https://doi.org/10.5194/tc-2020-109.
Kenner, R., Pruessner, L., Beutel, J., Limpach, P., Phillips, M., 2020. How rock glacier hydrology, deformation velocities and ground temperatures interact: examples from the Swiss Alps. Permafr. Periglac. Process. 31 (1), 3–14. https://doi.org/10.1002/ppp.2023.
Khadka, M., Kayastha, R.B. and Kayastha, R., 2020. Future projection of cryospheric and hydrologic regimes in Koshi River basin, Central Himalaya, using coupled glacier dynamics and glacio-hydrological models. Journal of Glaciology, https://doi.org/10.1017/jog.2020.51: 1-15. doi:https://doi.org/10.1017/jog.2020.51.
Khan, A., Naz, B.S., Bowling, L.C., 2015. Separating snow, clean and debris covered ice in the upper Indus Basin, Hindukush-Karakoram-Himalayas, using Landsat images between 1998 and 2002. J. Hydrol. 521, 46–64. https://doi.org/10.1016/j.jhydrol.2014.11.048.
Knight, J., Harrison, S., 2014. Mountain glacial and paraglacial environments under global climate change: lessons from the past, future directions and policy implications. Geografiska Annaler: Series A, Physical Geography 96 (3), 245–264. https://doi.org/10.1111/geoa.12051.
Leprince, S., Barbot, S., Ayoub, F., Avouac, J.-P., 2007. Automatic and precise orthorectification, coregistration, and subpixel correlation of satellite images, application to ground deformation measurements. IEEE Trans. Geosci. Remote Sens. 45 (6), 1529–1558. https://doi.org/10.1109/TGRS.2006.888937.
Lutz, A., Immerzeel, W., Shrestha, A., Bierkens, M., 2014. Consistent increase in High Asia's runoff due to increasing glacier melt and precipitation. Nat. Clim. Chang. 4 (7), 587. https://doi.org/10.1038/nclimate2237.
Lutz, A.F., Immerzeel, W., Kraaijenbrink, P., Shrestha, A.B., Bierkens, M.F., 2016. Climate change impacts on the upper indus hydrology: sources, shifts and extremes. PLoS One 11 (11), e0165630. https://doi.org/10.1371/journal.pone.0165630.
Marcer, M., Bodin, X., Brenning, A., Schoeneich, P., Charvet, R., Gottardi, F., 2017. Permafrost favorability index: spatial modeling in the French Alps using a rock glacier inventory. Front. Earth Sci. 5 (105). https://doi.org/10.3389/feart.2017.00105.
Marcer, M., Serrano, C., Brenning, A., Bodin, X., Goetz, J., Schoeneich, P., 2019. Evaluating the destabilization susceptibility of active rock glaciers in the French Alps. Cryosphere 13, 141–155. https://doi.org/10.5194/tc-13-141-2019.
Mayewski, P., Jeschke, P., Ahmad, N., 1981. An active rock glacier, Wavbal Pass, Jammu and Kashmir Himalaya, India. J. Glaciol. 27, 201–202. https://doi.org/10.3189/s0022143000011394.
Muhammad, S., Tian, L., 2016. Changes in the ablation zones of glaciers in the western Himalaya and the Karakoram between 1972 and 2015. Remote Sens. Environ. 187, 505–512. https://doi.org/10.1016/j.rse.2016.10.034.
Muhammad, S., Tian, L., Khan, A., 2019a. Early twenty-first century glacier mass losses in the Indus Basin constrained by density assumptions. J. Hydrol. 574, 467–475. https://doi.org/10.1016/j.jhydrol.2019.04.057.
Muhammad, S., Tian, L., Nüsser, M., 2019b. No significant mass loss in the glaciers of Astore Basin (North-Western Himalaya), between 1999 and 2016. J. Glaciol. 65 (250), 270–278. https://doi.org/10.1017/jog.2019.5.
Nicolsky, D.J., Romanovsky, V.E., Panteleev, G.G., 2009. Estimation of soil thermal properties using in-situ temperature measurements in the active layer and permafrost. Cold Reg. Sci. Technol. 55 (1), 120–129. https://doi.org/10.1016/j.coldregions.2008.03.003.
Nie, Y., et al., 2021. Glacial change and hydrological implications in the Himalaya and Karakoram. Nat. Rev. Earth Environ. 2 (2), 91–106. https://doi.org/10.1038/s43017-020-00124-w (In this issue).
Owen, L.A., England, J., 1998. Observations on rock glaciers in the Himalayas and Karakoram Mountains of northern Pakistan and India. Geomorphology 26 (1), 199–213. https://doi.org/10.1016/S0169-555X(98)00059-2.
Peng, C.-Y.J., So, T.-S.H., 2002. Logistic regression analysis and reporting: a primer. Underst. Stat. 1 (1), 31–70. https://doi.org/10.1207/S15328031US0101_04.
Rahman, M., et al., 2019. Flood susceptibility assessment in Bangladesh using machine learning and multi-criteria decision analysis. Earth Syst. Environ. 3 (3), 585–601. https://doi.org/10.1007/s41748-019-00123-y (In this issue).
Rahman, M., et al., 2021. Location-allocation modeling for emergency evacuation planning with GIS and remote sensing: a case study of Northeast Bangladesh. Geosci. Front. 12 (3), 101095. https://doi.org/10.1016/j.gsf.2020.09.022 (In this issue).
Rangecroft, S., Harrison, S., Anderson, K., Magrath, J., Castel, A.P., Pacheco, P., 2014. A first rock glacier inventory for the Bolivian Andes. Permafr. Periglac. Process. 25. https://doi.org/10.1002/ppp.1816.
Sattar, A., Goswami, A., Kulkarni, A. and Das, P., 2019. Glacier-surface velocity derived ice volume and retreat assessment in the Dhauliganga Basin, Central Himalaya-a remote sensing and modeling based approach. Frontiers in Earth Science, 7. doi:https://doi.org/10.3389/feart.2019.00105.
Sattler, K., Anderson, B., Mackintosh, A., Norton, K., de Róiste, M., 2016. Estimating permafrost distribution in the Maritime Southern Alps, New Zealand, based on climatic conditions at rock glacier sites. Front. Earth Sci. 4 (4). https://doi.org/10.3389/feart.2016.00004.
Scherler, D., Leprince, S., Strecker, M.R., 2008. Glacier-surface velocities in alpine terrain from optical satellite imagery—accuracy improvement and quality assessment. Remote Sens. Environ. 112 (10), 3806–3819. https://doi.org/10.1016/j.rse.2008.05.018.
Scherler, D., Bookhagen, B., Strecker, M., 2011. Spatially variable response of Himalayan glaciers to climate change affected by debris cover. Nature Geoscience, 4 https://doi.org/10.1038/ngeo1068.
Schmid, M.O., Baral, P., Gruber, S., Shahi, S., Shrestha, T., Stumm, D., Wester, P., 2015. Assessment of permafrost distribution maps in the Hindu Kush Himalayan region using rock glaciers mapped in Google Earth. Cryosphere 9 (6), 2089–2099. https://doi.org/10.5194/tc-9-2089-2015.
Schurer, A.P., Mann, M.E., Hawkins, E., Tett, S.F., Hegerl, G.C., 2017. Importance of the pre-industrial baseline for likelihood of exceeding Paris goals. Nat. Clim. Chang. 7 (8), 563–567. https://doi.org/10.1038/nclimate3345.
Scotti, R., Brardinoni, F., Alberti, S., Frattini, P., Crosta, G.B., 2013. A regional inventory of rock glaciers and protalus ramparts in the central Italian Alps. Geomorphology 186, 136–149. https://doi.org/10.1016/j.geomorph.2012.12.028.
Scotti, R., Crosta, G.B., Villa, A., 2017. Destabilisation of creeping permafrost: the plator rock glacier case study (central Italian Alps). Permafr. Periglac. Process. 28 (1), 224–236. https://doi.org/10.1002/ppp.1917.
Shrestha, M., Koike, T., Hirabayashi, Y., Xue, Y., Wang, L., Rasul, G., Ahmad, B., 2015. Integrated simulation of snow and glacier melt in water and energy balance-based, distributed hydrological modeling framework at Hunza River Basin of Pakistan Karakoram region. Journal of Geophysical Research: Atmospheres 120 (10), 4889–4919. https://doi.org/10.1002/2014JD022666.
Steiner, J.F., Kraaijenbrink, P.D., Jiduc, S.G., Immerzeel, W.W., 2018. Brief communication: the Khurdopin glacier surge revisited–extreme flow velocities and formation of a dammed lake in 2017. Cryosphere 12 (1), 95–101. https://doi.org/10.5194/tc-12-95-2018.
Wang, B., French, H.M., 1994. Climate controls and high-altitude permafrost, Qinghai-Xizang (Tibet) Plateau, China. Permafr. Periglac. Process. 5 (2), 87–100. https://doi.org/10.1002/ppp.3430050203.
Wester, P., Mishra, A., Mukherji, A., Shrestha, A., 2019. The Hindu Kush Himalaya. Mountains, Climate Change, Sustainability and People, Assessment https://doi.org/10.1007/978-3-319-92288-1.
Yang, M., Wang, S., Yao, T., Gou, X., Lu, A., Guo, X., 2004. Desertification and its relationship with permafrost degradation in Qinghai-Xizang(Tibet)Plateau. Cold Regions Science and Technology - Cold Reg Sci Technol 39. https://doi.org/10.1016/j.coldregions.2004.01.002.
Yao, T., Thompson, L., Yang, W., Yu, W., Gao, Y., Guo, X., Yang, X., Duan, K., Zhao, H., Xu, B., 2012. Different glacier status with atmospheric circulations in Tibetan Plateau and surroundings. Nat. Clim. Chang. 2 (9), 663. https://doi.org/10.1038/nclimate1580.
Yue, S., Pilon, P., Cavadias, G., 2002. Power of the Mann–Kendall and Spearman's rho tests for detecting monotonic trends in hydrological series. J. Hydrol. 259 (1), 254–271. https://doi.org/10.1016/S0022-1694(01)00594-7.
Zhu, H., et al., 2019. Trees record changes of the temperate glaciers on the Tibetan Plateau: Potential and uncertainty. Global Planet. Chang. 173, 15–23. https://doi.org/10.1016/j.gloplacha.2018.12.004.